Novel Tilting Ducted-Fan Aerial Vehicle Configurations

Larry A. Young
Aerospace Engineer
NASA Ames Research Center
Moffett Field, CA, USA

ABSTRACT

There has been recent renewed interested in ducted-fan, powered-lift vertical takeoff and landing aircraft vehicles for uninhabited aerial vehicle and urban aerial mobility aerial applications. Early work was conducted in the 1950's to the late 1980's into ducted-fan vehicles, especially at the time for military missions. The focus of ducted-fan research began to shift to UAV's and personal air transportation in the 2000's. Work in the early 2000's fostered interest into ducted-fan aerial vehicles for vertical lift planetary aerial vehicle missions, especially for missions to Titan, a moon of Saturn. For example, early work at NASA Ames conducted the first known investigation into oval ducts (with internal tandem fans) to be used for these aerial vehicles. The use of twin oval ducts (with internal tandem fans) allowed the use of quadrotor-style rotor rpm control for vehicle trim (in hover, for transition to high-speed forward flight the addition of a tilt-actuator to pitch the twin oval ducts forward to be aligned with the freestream needed to be added to the control approach. This current study explores open-rotor, single isolated ducted-fan, and full vehicle configuration aerodynamic performance for hover, transition, and cruise regimes for novel tilting ducted-fan aerial vehicle configurations. The objective of this study is to better understand the design aerodynamics trade space for noncircular tilting ducted-fans. The primary analysis tool used in this paper is the mid-fidelity computational fluid dynamics RotCFD tool. Several interesting and largely unexplored rotor-on-rotor (or fan-on-fan), duct-on-rotor, rotor-on-duct, and duct-on-airframe are examined in this paper. Many of these aerodynamic interactions are the key to overall aerial vehicle performance. Limited parametric sweeps of rotor-to-rotor spacing (and, therefore, sizing and shape of the enveloping ducts) for the various duct configurations will also be performed. The trade-offs between duct thrust augmentation in hover versus improved transition controllability versus improved cruise L/D will be discussed for various novel duct configurations. These ducted-fan configurations include oval ducts, 'figure-eight' ducts, and 'B-shaped' ducts, among others.

NOTATION

A	Rotor disk area, $A = \pi R^2$, m^2
c_{Duct}	Nominal (airfoil/cross-sectional) chord of duct, m
C_D^*	Duct (modified) drag coefficient, $C_D^* = D/q^*A$, nondim.
C_L^*	Duct (modified) lift coefficient, $C_L^* = L/q^*A$, nondim.
f	Duct fineness ratio, $f = \ell_D/2R_D$, nondim.
F_x	Duct-only longitudinal horizontal force, N
F_z	Duct-only vertical force, N
i_N	Nacelle, or rather duct, incidence angle, deg.; zero degrees with rotor axes vertical and 90 degrees with rotor axes are horizontal
L/D	Lift-to-drag ratio, nondim.
L/D_e	Effective lift to drag, L/D_e =WV/P, nomdim.
ℓ	Duct straight-line segment length (used in composite description of noncircular duct), m
ℓ_D	Nominal duct length, m
N_D	Number of ducts, nondim.
N_F	Number of fans (aka rotors), nondim.
N_{FPD}	Number of fans per duct, nondim.
N_{UDF}	Number of unducted fans, nondim.

Presented at the VFS Autonomous VTOL Technical Meeting, Mesa, Arizona, USA Jan. 24-26, 2023.

p	Duct circumferential perimeter, m
P	Total vehicle fan power, W
P_F	Fan (or rotor) power, W
q	Freestream dynamic pressure, $q = {}^1/_2\,\rho V^2$, N/m^2
q^*	Dynamic pressure that accounts for both freestream and fan induced velocities, $q^* = {}^1/_2\,\rho(v_h^2 + V^2)$, N/m^2
r_D	Duct circular arc radii (used in composite description of noncircular duct), m
R	Fan radius, m
R_D	Nominal duct radius, m
R_F	Nominal fan radius, m
S_D	Nominal duct reference area (circumferential perimeter of duct multiplied by nominal duct chord length), m^2
S_{DLS}	Alternate duct reference area (duct horizontal span multiplied by nominal duct chord length), m^2
t_D	(Airfoil/cross-sectional) thickness of duct relative to nominal chord of duct, m
T_{total}	Installed-in-duct total fan(s) thrust, N
V	Cruise velocity of vehicle, m/s
v_h	Hover fan ideal induced velocity, m/s
V_{Duct}	Duct volume, m^3
W	Weight of vehicle, Newtons
α	Angle-of-attack, deg.
χ	Thrust augmentation, $\chi = 1 + F_z/T_{total}$, nondim.
ϵ_{V_D}	Duct volume efficiency factor, $0 < \epsilon_{V_D} \leq 1$, nondim.
φ	Angular expanse of incremental circular arc segment partly comprising the composite noncircular duct geometry, Rad.
ρ_D^*	Duct structural density (in terms of duct 'planform' or, rather, exterior surface area), kg/m^2
ρ_D	Duct structural density, kg/m^3

INTRODUCTION

Vertical Takeoff and landing (VTOL) aircraft with tilting ducted-fans have been studied for decades. Among the noteworthy examples of tilting ducted-fan aircraft that have reached late stages of development have been the Doak VZ-4 (Ref. 1 and 2), the Bell X-22 (Ref. 3), and the Grumman 698 tilt-nacelle aircraft (Ref. 4). Interest in tilting ducted-fan aircraft continues to this day, including the recent Bell Nexus concept (Ref. 5). In addition to tilting ducted-fan aircraft configurations, there is a comparable body of interest in non-tilting ducted-fan aircraft such as the Airbus (Ref. 6) concept for urban air mobility (UAM) applications. Finally, the overall UAM, or eVTOL, development effort is quite extensive with many companies proposing a wide-ranging spectrum of vehicles, Ref. 7.

The relative advantages of tilting ducted-fan aerial vehicles versus other VTOL aircraft are multifold. These relative advantages (and disadvantages) are going to be dependent upon the application domains and mission profiles for the aircraft. The focus of this paper will be on the generic UAM mission profile as defined in Ref. 8. In the case of the notional UAM missions, tilting ducted vehicles can fly at higher, more efficient cruise speeds than edgewise rotor vehicle designs. In this regard, tilting ducted-fan vehicles have many of the same high-speed attributes as tiltrotor and tiltwing aircraft, as well as many of the emerging hybrid tilting-propeller vehicle designs from UAM aircraft developers. In the particular case of tilting ducted-fan vehicles versus tiltrotor aircraft, the tilting ducted-fan vehicle should have lower hover download than tiltrotors. Tilting ducts inherently are safer in terms of fans/rotors being shrouded by their ducts so as to avoid potential spinning rotor collision with people and objects; this attribute has an important positive subjective public acceptance impact. The relative disadvantages of tilting ducted-fan aerial vehicles versus other VTOL aircraft are: (1) increased vehicle weight to reflect the addition of large ducts, (2) potentially larger adverse ducted-fan and wing interference effects during all phases of forward flight versus tiltrotor proprotor/nacelle interference effects, and (3) potentially higher rotor downwash/outwash velocities than tiltrotors, tiltwings, and helicopters. Additionally, in particular, it should be emphasized that the relative advantages of tilting ducted-fan aerial vehicles versus fixed edgewise-flight ducted-fans are also dependent upon the missions to be accomplished. The advantages for a UAM type mission for tilting ducted-fan vehicles versus fixed edgewise-flight ducted-fan vehicles are: (1) more efficient and faster cruise operations, and (2) improved passenger acceptance because of greater separation distance of the fan blade-tips from the fuselage/cabin (as well as the visual and acoustic 'shielding' provided by the ducts themselves).

Most, if not all, tilting ducted-fan (aka tilt nacelle) aircraft design work has concentrated on the use of circular ducts. There are potential advantages and disadvantages of using noncircular ducts for such vehicles. Refer to Fig. 1 as to the

baseline vehicle and the circular and noncircular ducts studied in this paper.

Reference 9 was perhaps the earliest work to introduce the use of oval-shaped ducted-fans (with the fans in a tandem-like arrangement inside the ducts); it that regards it was among the first studies to begin to consider noncircular ducts in general for tilting ducted-fan aircraft. Reference 9 was focused on a small autonomous aerial vehicle to potentially fly on Titan, a moon of Saturn that has a dense atmosphere. However, despite that early planetary science mission focus, tilting ducted-fan aerial vehicles might find a broad range of mission application as, accordingly, sizes of vehicle. The focus of this paper will be on aircraft that can meet UAM mission requirements but, irrespective of that, tilting ducted-fan aerial vehicles might find any number of terrestrial 'drone' (aka UAVs, small autonomous aerial vehicles) applications as well.

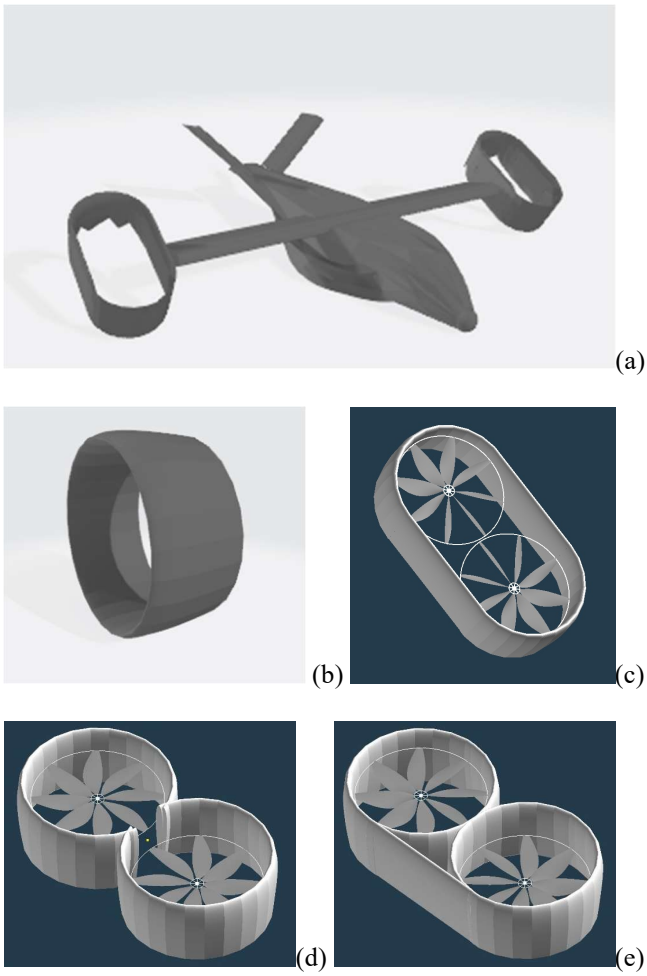

Figure 1. Baseline vehicle and circular and noncircular ducts studied in this paper: (a) complete vehicle with oval ducts; (b) isolated (single) circular duct; (c) close-up image of isolated oval duct with tandem fans; (d) 'Figure Eight' duct; (e) 'Figure Bee' B-shaped duct

This paper joins a similar body of work by the author on other aspects of urban air mobility and sustainable aviation, Refs. 10-14. Ultimately, the success of UAM is not just dependent on the successful development of aerial vehicles. It is truly a system-of-systems technical challenge that needs to address not just the vehicles but vertiport design, autonomous system technologies, electric-propulsion and recharging infrastructure, and automated air traffic management suitable for urban environments. Additionally, UAM support architectures need to support not only small passenger-carrying vehicles on on-demand and/or scheduled service but also need to support smaller rotary-wing and VTOL UAVs/drones and well as potentially fixed-wing UAVs that might also be flying in the urban environment.

INTRODUCTION OF CONFIGURATIONS AND FIRST ORDER (ALL-ELECTRIC) CONCEPTUAL DESIGN SIZING

NASA has invested in the past five years or more a considerable amount of effort examining the conceptual design trade space for aerial vehicles that could potentially meet the emerging urban air mobility application domain. This effort has been especially focused on vehicles with all-electric or hybrid-electric propulsion systems. Representative UAM mission profiles have very short total mission ranges and, therefore, electric propulsion seems to be viable for such missions in a reasonable developmental time frame. Though defining NASA vehicle reference designs is a big part of the overall NASA effort, the work has tended to be dominated by the development of robust, reliable, and relatively computational/time efficient analysis tools and processes to perform conceptual and preliminary design efforts by the Government, Academia, and Industry.

The novel tilting ducted-fan configurations presented in this paper represents both a new set of opportunities to define new vehicle reference designs as well as defining/considering new enabling technologies to be developed in the future by NASA to aid in the further advancement of the UAM application domain.

General Vehicle and Duct Configurations Studied

Figure 1a-e are the vehicle and ducted-fan configurations studied in this paper. For the most part, only tilting ducted-fan vehicles with two wing-mounted ducts are considered in this paper, i.e. vehicle configurations similar to the Doak VZ-4 (e.g. refer to Refs. 1-2) but with mostly noncircular ducts. A baseline set of cases for isolated circular ducts (with both a single fan and coaxial fans, refer to both Fig. 1b and Fig. 2b) and a complete vehicle with circular ducts (Fig. 2a) were generated as baselines to compare against the noncircular duct results.

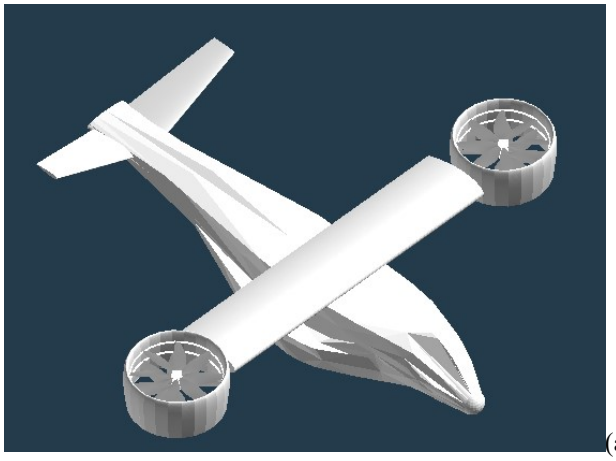

(a)

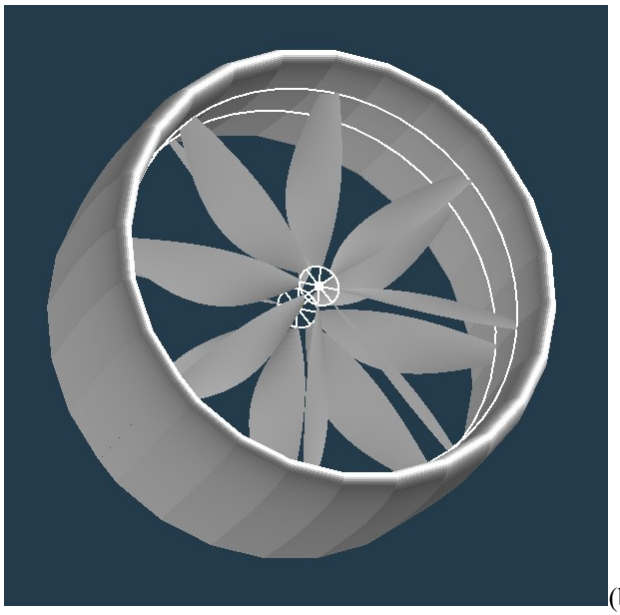

(b)

Figure 2. Circular ducted-fan baseline: (a) vehicle configuration and (b) isolated single duct (with coaxial fans)

General Sizing Model Consideration for Novel Tilting Ducted-Fan Aerial Vehicles

There are two primary focus areas to consider in improved general models for tilting ducted-fans aerial vehicles for conceptual design sizing analyses. First, unique weight equations for circular and noncircular ducts need to be developed. Second, first order aerodynamics models to account for fan-on-duct, duct-on-fan, and wing-on-duct interference effects are also needed. Chief among these aerodynamic interference effects: (1) fan thrust augmentation in hover and low-speed flight and (2) wing-on-duct increased parasite drag during cruise. Additionally, there is another set of aerodynamics concerns for wing-mounted tilting ducted-fan configurations in transition (from helicopter- to airplane-mode).

In order to make sizing estimates of tilting ducted-fan aircraft it is necessary to make estimates of duct (outer) surface area, volume, and weight. All three parameters can be derived from estimates of the nominal circumferential perimeter of the duct inlet. This perimeter, p, estimate is highly dependent on the noncircular shape of the duct. For circular ducts the perimeter, is a simple expression, Eq. 1. For a composite noncircular duct, the duct perimeter is given by Eq. 2.

$$p_{Circular\ Duct} = 2\pi R_D \tag{1}$$

It is assumed for the noncircular duct shapes studied in this paper, that the overall shape is a composite of straight-line segments and circular arcs.

$$p = \sum_{i=1}^{M} \ell_i + \sum_{j=1}^{N} \varphi_j r_{D_j} \tag{2}$$

In turn, the nominal duct reference area, S_D, is given by Eq. 3.

$$S_D = pc_{Duct} \tag{3}$$

The duct volume, V_{Duct}, can be approximately given by Eq. 4, where for the purposes of the sizing analysis, $\epsilon_{V_D} \approx 0.5$.

$$V_{Duct} \approx t_D S_D \epsilon_{V_D} \tag{4}$$

The total weight of all ducts (all ducts assumed to be identical) is given by Eq. 5.

$$W_{Ducts} = N_D \rho_D V_{Duct} \tag{5}$$

An alternate (perhaps more conventional) approach is to define the duct weight as such

$$W_{Ducts} = N_D \rho_D^* S_D \tag{6}$$

Parameter ρ_D^* is given the value of 14.6kg/m^2 (3lbf/ft^2); which is consistent with the method and value used in Ref. 15.

In both Eqs. 5-6, the number of ducts is given by Eq. 7.

$$N_D = (N_F - N_{UDF})/N_{FPD} \tag{7}$$

As an example, an oval duct with ~2R (more precisely, R+R_D) fan-to-fan longitudinal spacing can be defined in the composite geometry manner as follows in Eq. 8a-c.

$$\ell = \begin{bmatrix} R + R_D \\ R + R_D \end{bmatrix} \qquad \varphi = \begin{bmatrix} \pi \\ \pi \end{bmatrix}$$

$$r_D = \begin{bmatrix} R_D \\ R_D \end{bmatrix}$$

(8a-c)

As a miscellaneous analysis to finish off this modeling section, the duct (exhaust expansion area) ratio can be given (for a symmetrical airfoil-type duct cross-section) as shown in Eq. 9.

$$\frac{A_e}{A_F} \approx (1 + f t_D)^2$$

(9)

Where f is the duct fineness ratio is given by $f = \ell_D / 2R_D$. Equation 9 assumes that one of the fans in the duct is located at a vertical station coincident with the maximum thickness (chordwise) location of the airfoil-type duct cross-section. The larger the duct area ratio is the greater theoretical exhaust expansion and increased exhaust thrust augmentation (versus thrust augmentation stemming from suction pressure on the duct lip/rim due to entrained/induced flow from the embedded fans in the duct.

During cruise, the incremental drag contribution from ducts can be approximately given by

$$\Delta D = c_{d0} q S_D$$

(10)

Where c_{d0} is the zero-lift sectional drag coefficient for the duct airfoil/cross-sectional contour; c_{d0} for a NACA 0012 (tripped) is ~0.008.

During transition, simplified first order formulas (based on modification/hybridization of Newton's sine squared normal force expressions for high angles of attack flat plate flow).

$$\Delta D_{Duct} = \left[c_{d0_{Duct}} sin(i_N) + 2\delta sin(\pi/2 - i_N)^3\right] q^* S_{DLS}$$

$$\Delta L_{Duct} = [\delta_1 cos(i_N) + 2\delta sin(\pi/2 - i_N)^2 cos(\pi/2 - i_N)] q^* S_{DLS}$$

(11a-b)

Where S_{DLS} an alternate duct reference area used in this modeling, which is the total effective horizontal span of the duct divided by the nominal duct chord length. For an oval duct, $S_{DLS} = 4R_D c_{Duct}$. Note δ and δ_1 are an empirical correction factor; for the sizing work presented in Tables 1-5, a value of $\delta = 1$ was used. The parameter δ_1 captures the duct thrust augmentation due to the suction pressure on the duct rim/lip that is generated by the fan induced velocity at the duct inlet; δ_1 is approximately a constant and, for purposes of the sizing analysis performed in this paper, $\delta_1 = 0.4$. (By simple dimensional analysis, it follows that $\Delta L_{Duct} \propto T_{total}$ and in hover $q^* \propto T_{total}$; therefore, given the functional form of Eq. 11b, $\delta \propto constant$.) Note that the duct/nacelle incidence angle has been converted to radians in the above equation.

Sizing of Novel Ducted-Fan Configurations

NASA has performed some recent UAM conceptual design work with respect to tilting ducted-fan vehicles (Ref. 15). This work primarily focused on a six-duct (with circular ducts) vehicle with each duct having a single fan embedded in them and, further, each duct had control vanes also incorporated into the ducts. The work described in this paper deviates from the Ref. 15 work in that the focus is on noncircular ducts with coaxial or tandem fan arrangements embedded in the ducts. Further, it is assumed that only two ducts (mounted at the wingtips of a single main wing) are employed on the vehicle(s).

It is assumed in the sizing analysis presented in this paper that all fans and ducts are of the same size and geometry. This is not an absolute; it can be readily imagined that a heterogeneous array of fan and duct sizes and geometries might be employed in a single aircraft design, but that is not what is assumed in the following analysis.

For the presented sizing estimates, it is assumed that the vehicles have all-electric propulsion using batteries. Alternate propulsion systems could be considered such as hybrid-electric (for different combinations of battery versus direct current supply from a turbogenerator), and an internal combustion engine (ICE) or turboshaft engine. An all-electric configuration is chosen for this study because arguably it is the propulsion type most often proposed for UAM missions and is most consistent with current aviation sustainability goals. Sizing for an all-electric vehicle does increase the challenge of arriving at design closure even for the UAM mission profile. Consequently, this yields heavier vehicles than a hybrid-electric or turboshaft-driven propulsion system.

All other vehicle weight group estimates are based on either Ref. 14 regression analysis methodology derived from a set of tiltrotor aircraft conceptual designs from Refs. 16-19 or are based on the well-known sizing methodologies (principally for the rotor and controls groups) of Refs. 20-21. Note that the controls weight estimates for the tilting duct fan vehicles have been reduced with a knockdown factor to reflect that only collective, not cyclic control, is being employed for rotor control. A recent well-known rotorcraft sizing tool is Ref. 22;

note that the Ref. 22 sizing tool was used for the Ref. 22 ducted fan study.

A duct thrust augmentation factor of 1.4 is assumed for the following sizing study; this magnitude of thrust augmentation has been observed experimentally for circular ducts, including Ref. 9. This thrust augmentation captures the effect of both duct inlet suction pressure as well as duct diffuser/exhaust expansion. Note that noncircular duct geometries might affect the thrust augmentation factor but for the purpose of this initial sizing study the thrust augmentation factor is held constant at 1.4. Later in this paper, mid-fidelity computational fluid dynamics (CFD) work will begin to better capture the influence of noncircular geometry on duct thrust augmentation.

Four different tilting ducted-fan configurations were sized by a simple spreadsheet-type sizing analysis: (1) a circular duct with coaxial fans embedded in the ducts; (2) an oval duct (with tandem fans embedded in the ducts); a 'Figure Eight' shaped duct (with tandem fans); and a 'Figure Bee' shaped duct (with tandem fans). Note that there is a parametric spectrum of different oval, Figure Eight, and Figure Bee shaped ducts. The nominal 'baseline' noncircular duct configurations (discussed in more detail below but, overall, having a longitudinal fan-to-fan separation of 2R to 2.1R) are what are used in the below vehicle sizing. A representative result for a vehicle having Oval ducts (2 radii longitudinal spacing for the tandem fans embedded in the ducts) is summarized in Table 1. A loose convergence tolerance of a half-percent on vehicle takeoff gross weight was employed in this initial study. The loose convergence tolerance was used to reflect the low fidelity of some of the sizing methodology employed. A constant duct chord length of $c_{Duct} = 0.35R$ was used in this study; this low chord length ratio was chosen to keep duct weights to a minimum, to get sizing closure. Duct geometries studied later in the paper with mid-fidelity CFD had a larger duct chord length ratio. Future work will have to consider more closely the impact of duct chord length on the vehicle aerodynamics and weight estimates. Note that a tech factor of 0.65 was applied to the duct weight estimates; duct weight was estimated in a similar manner as Ref. 15, with the same tech factor and structural density value being used for both this paper's study and Ref. 15.

There is a small sensitivity of vehicle takeoff gross weight – for all-electric (batteries only) vehicles – on duct reference surface area (and, therefore, duct mass). Tripling the duct reference area results (with the circular duct having the lowest reference area and the Figure Bee duct having the highest reference area) in a twenty-percent increase in vehicle takeoff gross weight; refer to Fig. 6. Future work should consider the implications of using hybrid-electric propulsion system (or solely turboshaft engines) for tilting ducted-fan aerial vehicles. There is a likelihood that the sensitivity of vehicle gross weight on duct size and geometry (and weight) will be reduced for other types of propulsion as compared to all-electric, battery propulsion. The following battery characteristics are assumed for the sizing study: power density of 670 W/kg (from Ref. 11) and an energy density of 400 Wh/kg (from Ref. 23). All batteries ended up being sized by their power output characteristics versus their energy storage capacity.

This work is very preliminary and of first order. Simple aerodynamic models are used in the sizing analysis – especially for the climb and transition segments of the mission profile – have first order modeling fidelity. Much of the mid-fidelity CFD work noted later in the paper has not been incorporated in the sizing analysis yet. This is left to future work.

Table 1. Oval Ducted-fan (~2R longitudinal fan-to-fan spacing) Vehicle ($S_D = 13.5m^2$)

Main Rotor Disk Loading	965.21551	N/m^2
Main Rotor Radius	1.3515569	m
Number of Blades	8	Nondim.
Main Rotor Solidity	0.2	Nondim.
Main Rotor Tip Speed	183.762	m/s
Nominal (Mean) Airplane-Mode Cruise Wing Loading	5147.839	N/m^2
Cruise Wing (Including Duct Planform) Area	11.533782	m
Number of Electric Motors per Rotor	1	Nondim.
Hover Power	641.0735	kW
Advance Ratio	0.1259771	Nondim.
Nominal Helicopter-Mode Forward Flight Power	703.78119	kW
Vehicle Effective Lift over Drag in Airplane-Mode Cruise	6.9016386	Nondim.
Nominal (Mean) Airplane-Mode Cruise Power	340.02001	kW
Payload	545.45455	kg
Total Weight of Rotors	183.6772	kg
Fuselage Weight	303.33136	kg
Wing Weight	332.38573	kg
Total Turboshaft Engines, turbo-generator, Drive Train We	0	kg
Total Fuel Weight	0	kg
Total Battery Weight	1050.4197	kg
Total Electric Motor Weight	373.30144	kg
Total Fixed Equipment Weight	124.58588	kg
Total Tilting Duct System Weight	175.83904	kg
Total TOGW =	3088.9949	kg

Note that in Table 1, TOGW is an acronym for takeoff gross weight; the term design gross weight is used equivalently to TOGW in Fig. 3.

Figure 3 summarizes tilting ducted-fan vehicle (and select systems) design gross weight growth as a function of (single) duct reference area, which is the duct circumferential 'perimeter' multiplied by the mean duct chord length. The lowest design gross weight vehicles are those that use circular ducts followed by those vehicles that use Oval, then Figure Eight, and, finally, Figure Bee ducts. Mid-fidelity computational fluid dynamics work summarized later is this paper will examine the influence of duct geometry on ducted-fan 'thrust augmentation' in hover and, therefore, revisit the assume thrust augmentation factor (a value of 1.4) used, in part, to generate the Table 1 and Fig. 3 sizing results.

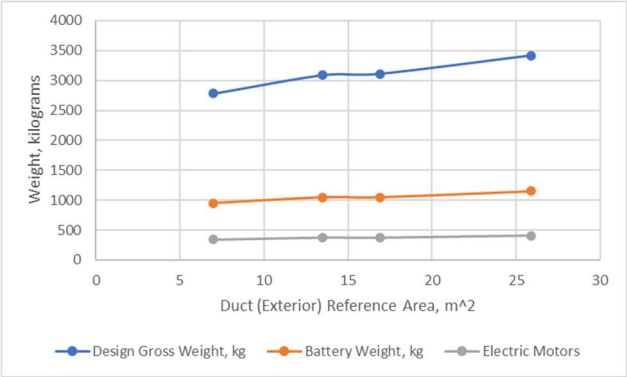

Figure 3. The influence of duct (Exterior) reference area (for a single duct) on tilting ducted-fan vehicle and select system weights

There is tradeoff between duct size and geometry (resulting in greater duct weight and, therefore, vehicle takeoff gross weight) versus the potential simplicity and robustness of control in hover and low-speed forward flight.

Noncircular ducts result in heavier aircraft as demonstrated in Fig. 3. This weight growth is moderately large for all-electric aircraft; it is anticipated that turboshaft-engine or hybrid-electric aircraft would be less sensitive to duct weight. Further, these results suggest that the modest disk loading aircraft sized in this study most likely should be updated with higher disk loaded aircraft to keep the ducts smaller and the duct weight less. This, of course, has its own set of challenges, such as higher fan outwash velocities, noise (without sound attenuation from the ducts), and reduced low-speed pitching-moment control with a differential thrust only control approach (no control vanes in the duct wake).

BASIC FLIGHT CONTROL CONSIDERATIONS FOR NOVEL TILTING DUCTED-FAN CONFIGURATIONS

The common feature for almost all the novel tilting ducted-fan aerial vehicle configurations described in this paper is that differential thrust between fore and aft pairs of fans (embedded in the same duct) can be used to effect low-speed pitching-moment control for the aircraft. Further, differential thrust between side-by-side pairs of fans (between two wing-mounted ducts) can control roll-moment and yaw-moment. In this regards, low-speed control for most of the novel tilting ducted-fan configurations studied in this paper can be considered similar in nature to the type of differential thrust control seen for quadcopters/quadrotors and/or other multirotor vehicle configurations typically seen for UAVs/drones. For low-speed control for both types of vehicles (the novel tilting ducted-fan vehicles discussed in this paper and multirotor UAVs/drones), differential thrust can be achieved by collective control inputs and/or fan/rotor rpm speed changes. However, even in low-speed flight, the longitudinal fan-to-fan separation may be inadequate to allow robust pitching-moment control, especially if missions require a large range of center-of-gravity locations in the aircraft. In that case, fan differential thrust control must be augmented by the addition of actuated vanes in the duct to provide variable angle settings for additional pitching-moment.

It is anticipated that the fans in these proposed novel tilting ducted-fan configurations have variable pitch/collective but no cyclic control. Obviously, this is a design choice that can be reexamined as vehicle designs mature. For now, though, it is assumed for simplicity that there is only collective control for all fans. Therefore, in transition and cruise, the vehicle would operate in more of a similar manner as a tiltwing aircraft, with vehicle pitching-moment control balanced between main-wing flaperon control and tail-surface elevator control.

DUCT/VEHICLE AEROPERFORMANCE PREDICTIONS

The aeroperformance work presented in this paper is based on mid-fidelity computational fluid dynamics predictions. The computational fluid dynamics software used throughout this paper is the RotCFD code developed by the late Prof. R. Ganesh Rajagopalan of Iowa State University and Sukra-Helitek under partial NASA sponsorship (Ref. 24-25). The rotors in this work are represented as actuator disk, distributed momentum sources. (RotCFD also has the capability of modeling the rotors as effectively lifting-line representations, but that capability was not used for the results presented in this paper.)

Isolated Ducted-Fan Hover and Forward Flight Trends

All the fans modeled in the study are generic in nature. The fans are eight-bladed, with a tip speed of 183m/s (600 ft/s) and a nominal rotor radius of 1.83 meters (six feet). The rotor rigid coning angle is one degree, the rotor cutout is 0.1R, and a uniform NACA 0012 airfoil is used across the rotor blade span. The rotor blade twist and chord distributions are shown in Fig. 4a-b. This fan geometry was selected early in the study and was not informed by the aircraft sizing analysis presented above; therefore, the following ducted-fan and vehicle CFD modeling should be considered in the context of a generic parametric trade study. (For additional code-specific modeling details related to the RotCFD predictions, a rotor refinement of nine was consistently used for all predictions and a 'refinement box' refinement of six was also consistently used for all predictions). Standard density, temperature, and pressure, and dynamic viscosity for air at sea-level was used in the predictions.

All the ducts are defined as bodies of revolution using a NACA 0012 as the cross-sectional contour for the duct. The fineness ratio (duct diameter to duct length) used for the circular-ducts (and the circular arc segments of the noncircular ducts studied) is constant and is f=0.49. The same fan-to-fan vertical spacing ratio ($\Delta z/R=0.29$ or $\Delta z/c_{duct} = 0.27$), and the relative location of the upper/aft fan to the duct inlet rim/lip ($z_{lip}/R=0.28$ or $z_{lip}/c_{duct} = 0.26$) was also kept constant throughout the duct studies.

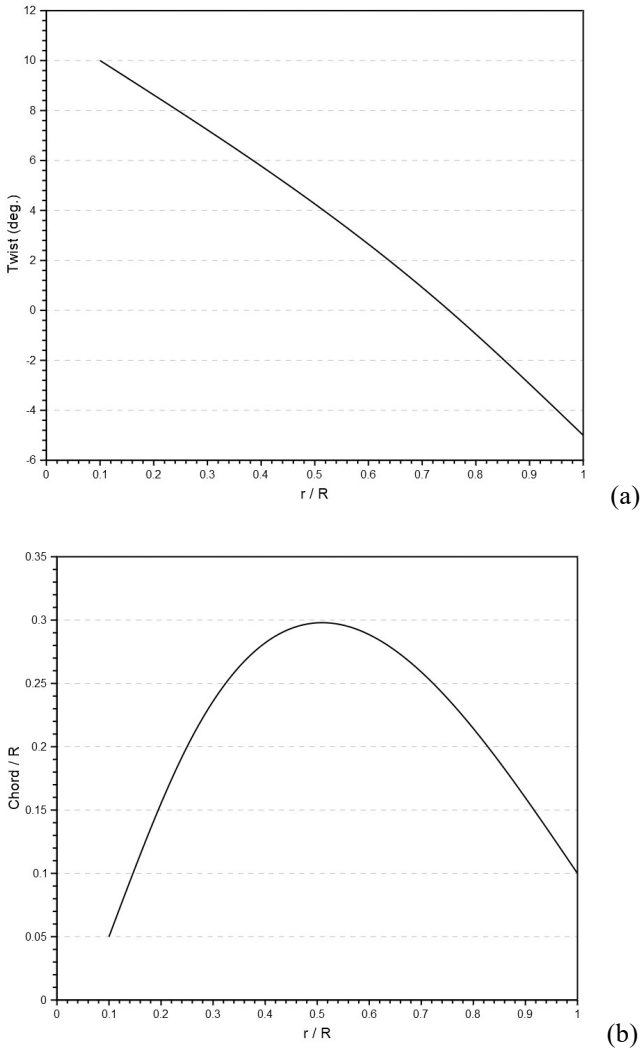

Figure 4. Fan blade (a) twist and (b) chord distributions used for all tilting ducted-fan modeling used in this paper

The intent is not to present an optimal fan geometry but instead a common generic fan model to perform preliminary studies of alternate (noncircular) duct geometries. Relatively low disk loadings (~ 960 N/m^2 or ~20psf) for the fans are studied. This low disk loading is potentially a major design issue to consider more fully in the future. Most historical work with ducted-fans has been at much higher disk loadings. Low disk loading fans were studied in this paper to be more consistent with other NASA UAM reference designs, including that of Ref. 15. Higher fan disk loading, though, would result in smaller fans and, therefore, less duct weight, even if there was a corresponding reduction in fan efficiency because of the higher disk loading. As was seen in the sizing analysis section of the paper, reducing duct weight will be an important consideration in future work with both circular and noncircular tilting ducted-fan aerial vehicles, especially those designs relying on all-electric battery propulsion systems.

Figure 5 illustrates the typical near-field gridding used in the mid-fidelity CFD tool used in this study. Figures 6-8 present hover flow field CFD predictions for various 'baseline' isolated open-rotors and fans-in-duct configurations: an Oval duct of 2R longitudinal span, a "Figure Eight" configuration of 2.1R longitudinal span, and a "Figure Bee" configuration of 21.R longitudinal span. (Later work will perform some configuration geometric/parametric sweeps/deviations from these 'baseline' duct configurations.) The isolated ducted-fan predictions are made with medium-fineness CFD gridding (for the RotCFD software tool, Refs, 24-25, this is expressed in terms of rotor, body, and off-body refinement levels; rotor refinement of nine, body refinement of eleven and/or twelve, and an off-body, aka refinement box, refinement of six). A cartesian off-body grid is used with body fitting for the near-body-surfaces. Not that there can be both a longitudinal and vertical separation between the two rotors/fans embedded in the various ducts (some limited single fan in circular duct predictions are also presented for general reference; the focus is on coaxial (equivalent to zero longitudinal separation) and tandem fan arrangements.

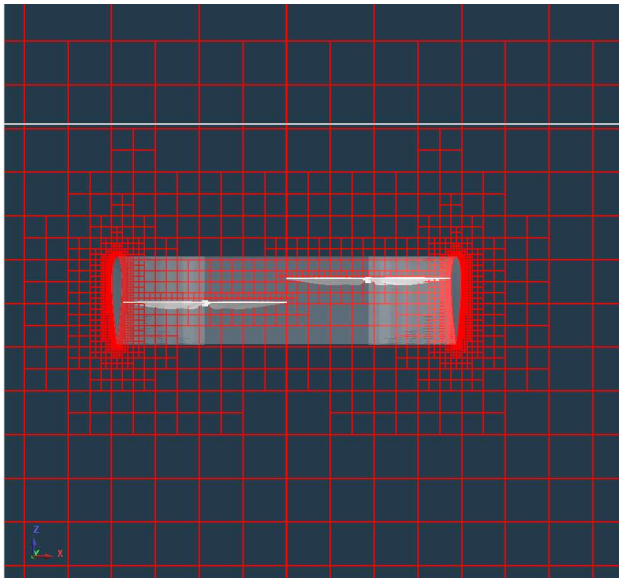

Figure 5. Representative CFD gridding for RotCFD for isolated ducted-fans in hover conditions (in this particular case an Oval duct)

No internal support structure, cross-shafting, or direct-drive electric motors are modeled in this current study. Only the rotors and the duct are modeled for most of the isolated ducted-fan configuration results. (Later in the paper a brief introduction/discussion of these miscellaneous aerodynamic

effects, including that of the introduction of actuated vanes inside the duct for improved pitching-moment control, will be briefly discussed.)

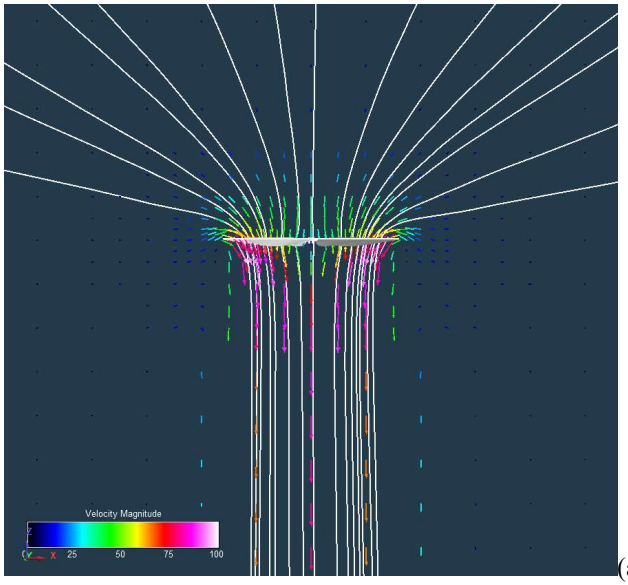

(a)

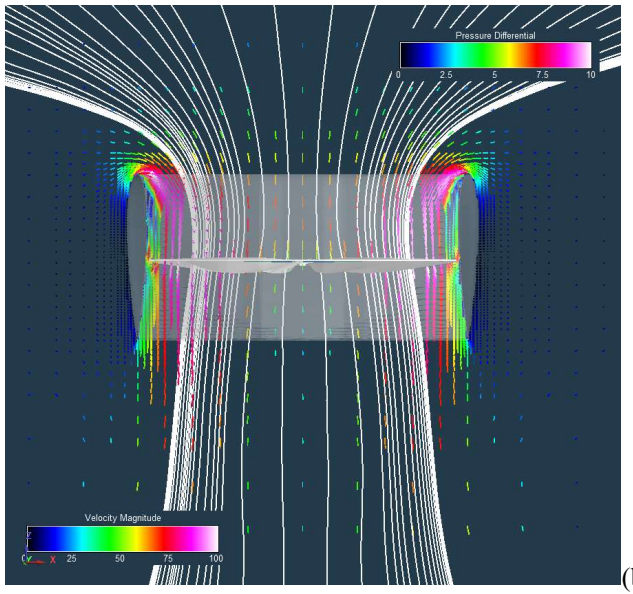

(b)

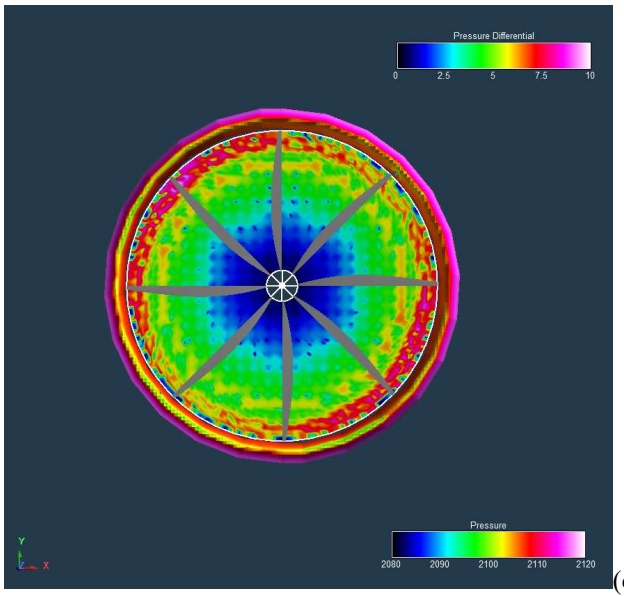

(c)

Figure 6. Hover flow field predictions (Collective=15 deg.) for open-rotor and fan-in-duct configurations: (a) single open rotor, (b) side view of circular ducted-fan with single rotor/fan, and (c) top view of circular ducted (single) fan

Comparing Fig. 6a isolated rotor/fan streamlines with Fig. 6b single fan circular ducted-fan streamlines clearly shows the expected ducted-fan diffuser/exhaust wake expansion downstream of the duct outlet. The duct exhaust wake expansion, or 'jet,' contributes (in addition to the duct inlet rim/lip suction pressure contribution) to the overall fan 'thrust augmentation' in hover. Figure 7a to Fig. 7b demonstrates a similar duct wake expansion for coaxial fans as well seen in the single fan results of Fig. 6a-b. The fineness ratio of the duct for CFD predictions is f= 0.49; note, the fineness ratio used in the sizing analysis was much lower, f=0.16, because of duct weight reduction considerations.

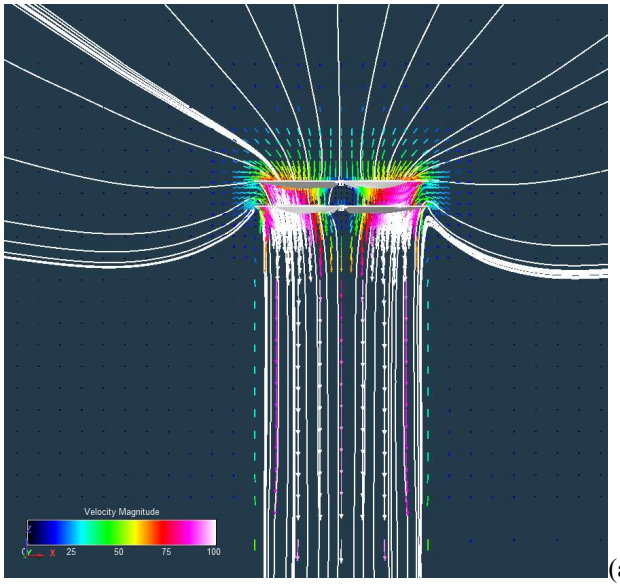

(a)

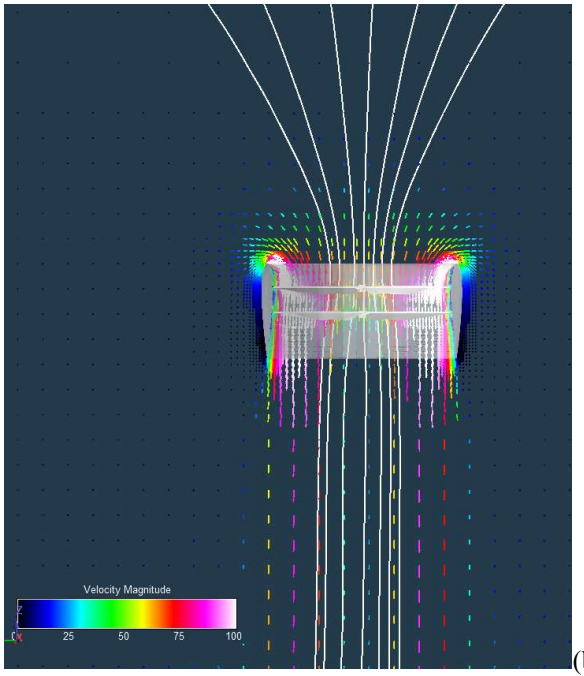

(b)

Figure 7. Hover flow field predictions (Collective=15 deg.) for open-rotors and fans-in-duct configurations: (a) coaxial open rotor and (b) circular ducted-fan with coaxial rotors

Figure 8a-d presents hover flow field results (collective of 15 deg.) for an open-rotor tandem fan arrangement and the corresponding baseline isolated (i.e. single) ducted-fan configurations. In addition to the flow field velocity vectors on a plane through the fan rotational axes, also shown are the rotor differential pressure across the rotor disks as well as duct surface pressures. Having both open-rotor and ducted-fan sets of predictions enables the ability to quantify duct-on-fan and fan-on-duct aerodynamic interactions in hover.

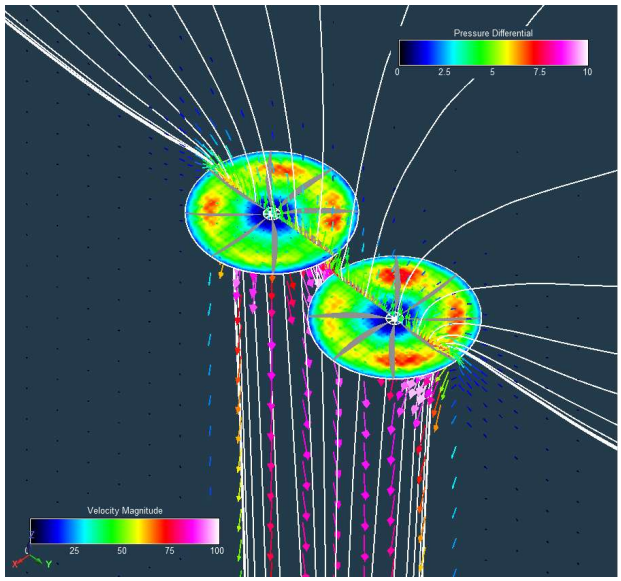

(a)

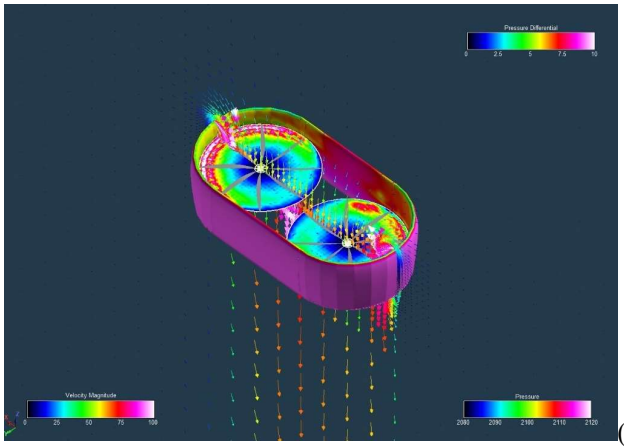

(b)

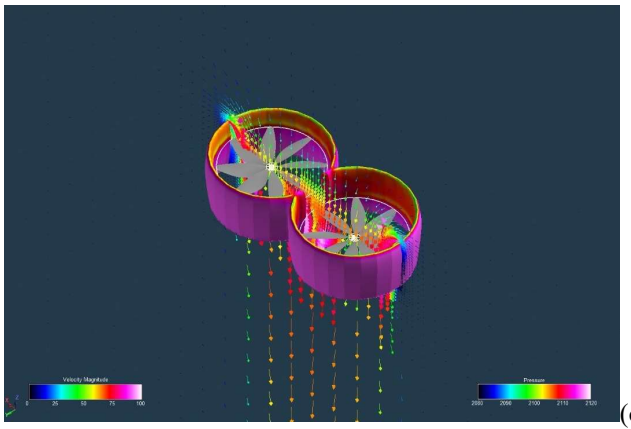

(c)

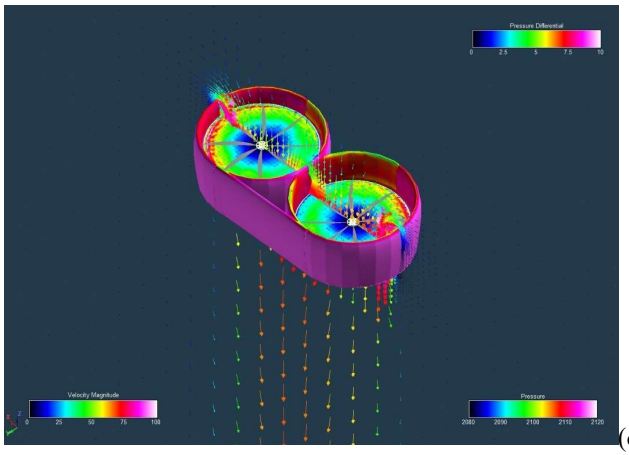

(d)

Figure 8. Hover flow field predictions (Coll.=15 deg.) for open-rotors and fans-in-duct configurations: (a) tandem open rotors; (b) oval ducted-fan; (c) 'Figure Eight' ducted-fan; (d) 'Figure Bee' B-shaped ducted-fan

Figures 9-12 results would suggest that there is little difference between the two open rotor configurations (isolated, single fan and the tandem fan arrangement) in hover. The mean thrust and power coefficients for the single isolated rotor configuration, versus the tandem open-rotor configuration (2R longitudinal separation between rotor axes with a 0.29R vertical spacing) are approximately equivalent trend-wise. On the other hand, considering only the mean

rotor thrust and power coefficient – and not including duct contributions to the thrust (i.e. the net vertical force from the duct rim/lip suction pressure) – ducts of the four types studied all seem to have a similar adverse impact on hover performance. Note that the circular duct with a single fan seems to suggest premature fan blade stall given the slight flattening out of thrust with collective and the increase in power at the 25Deg, collective setting. The tip loss factor used in the RotCFD mid-fidelity CFD analysis (wherein the fans are represented as distributed momentum sources, equivalent to 'actuator disks') is a unform value for all predictions in this paper of 0.95. (A tip loss factor is a well-known approach to account for the three-dimensional flow at rotor blade tips and to account for the corresponding loss of lift at those tips due to the three-dimensionality of the tip flow.) It may be, though, that a tip loss factor appropriate for open rotors/fans might not be appropriate for fans in ducts. This is something worthy of future investigation.

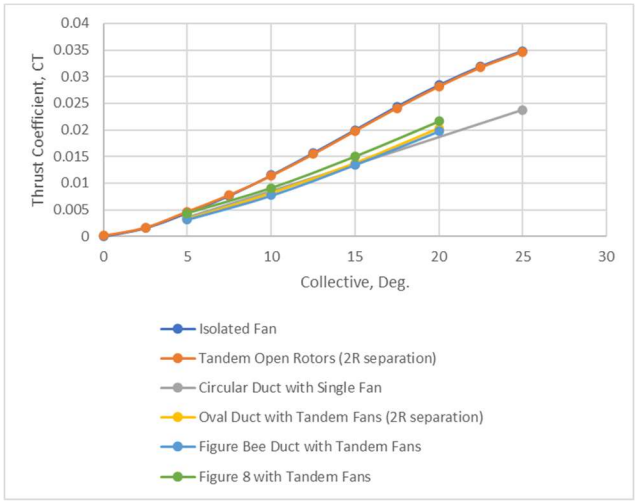

Figure 9. Fan collective sweeps for hover rotor (only) thrust for open-rotors and fans-in-duct configurations

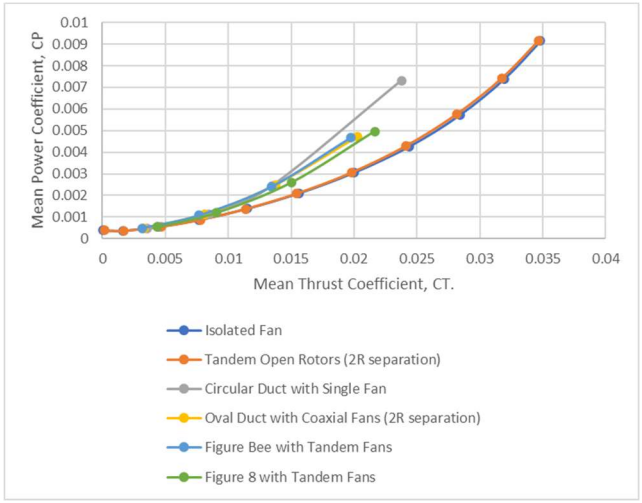

Figure 10. Hover rotor (only) thrust and power polar for open-rotors and fans-in-duct configurations

A hover thrust augmentation effect can be clearly seen in Figs. 18-19. Note that the definition of hover thrust augmentation used throughout this paper is $\chi = 1 + F_z/T_{total}$.

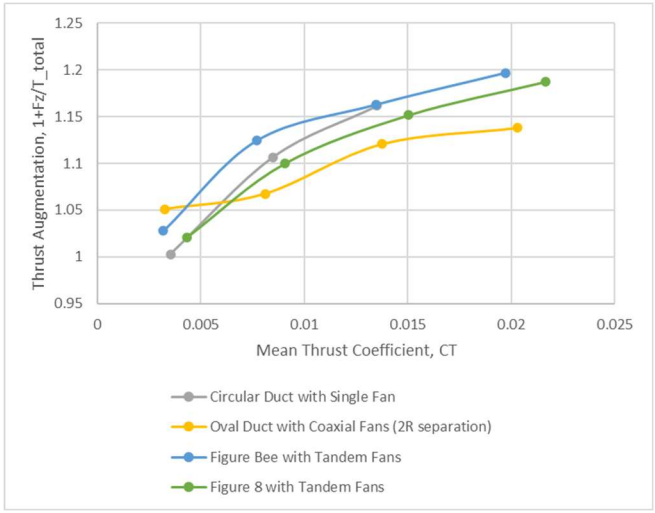

Figure 11. Thrust augmentation effect (with the combined fans(s) and duct thrust and vertical force) as a function of mean rotor thrust coefficient

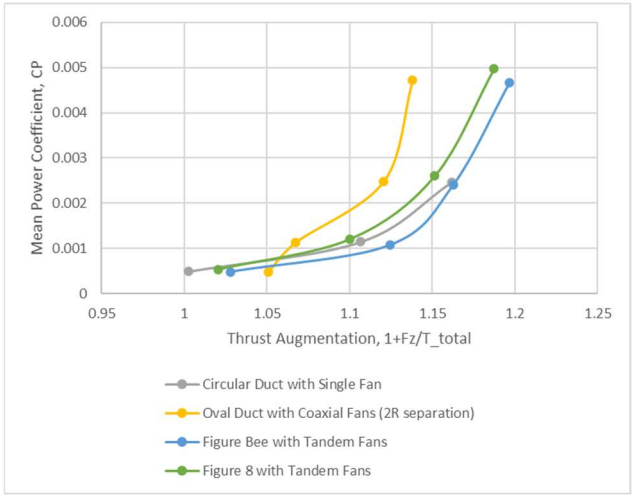

Figure 12. Thrust augmentation effect (with the combined fans(s) and duct thrust and vertical force) as a function of mean rotor thrust coefficient

The thrust augmentation predicted by the mid-fidelity CFD tool are less than what has been typically reported in the literature for ducted-fans (i.e. thrust augmentations ~ 1.4). Then again, most of the reported ducted-fan work has been at higher disk loading than modeled in this paper. The CFD results seem to confirm that higher thrust augmentation occurs with higher fan disk loading. A circular duct, from purely a hover thrust augmentation perspective seems to be a slightly better geometric configuration than the Figure Eight and Figure Bee configurations.

Figures 13-15 consider the transitional and cruise phases of forward flight for isolated open-rotors and fans-in-duct configurations. Even for the isolated ducted-fan predictions, in transition the flow fields about the ducts are very three-dimensional. This holds true for all duct shapes considered in this study. The high degree of three-dimensionality is a cautionary note to ducted-fan aircraft aerodynamicists and designers to be careful in not relying on oversimplified assumptions and analysis for these vehicles, especially in the transition flight regime.

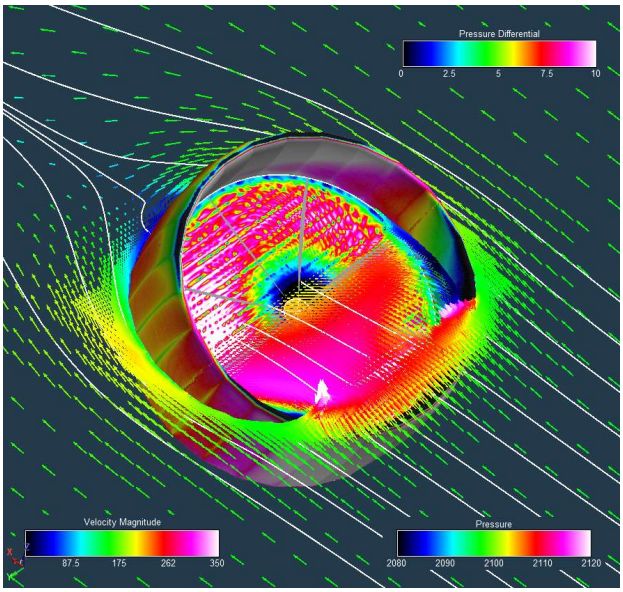

Figure 13. Flow field predictions of the 'baseline' single-fan, circular ducted-fan configuration; freestream velocity of 46 m/s (150 ft/s), collective of 45 deg., nacelle incidence angle of 30 deg.

It appears that the use of the composite geometry approach to define ducts, including the circular ducts, has introduced some gridding issues that occasionally has resulted in non-watertight CAD geometries and, therefore, some adverse flow artifacts where some internal flow in the interior of the duct fairings. This effect is generally small on the CFD performance results but can result in some artifacts in the duct surface pressures. A secondary geometry issue is the appearance of 'chine' edge artifacts around the circumference of the outer and inner surfaces of the ducts. These 'chine' artifacts can be observed to also have an impact of the duct body surface pressures.

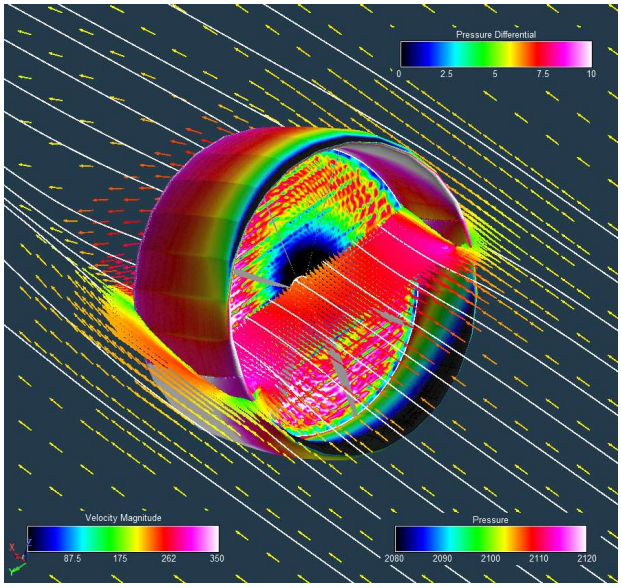

Figure 14. Flow field predictions of the 'baseline' single-fan, circular ducted-fan configuration; freestream velocity of 61 m/s (200 ft/s), collective of 45 deg., nacelle incidence angle of 60 deg.

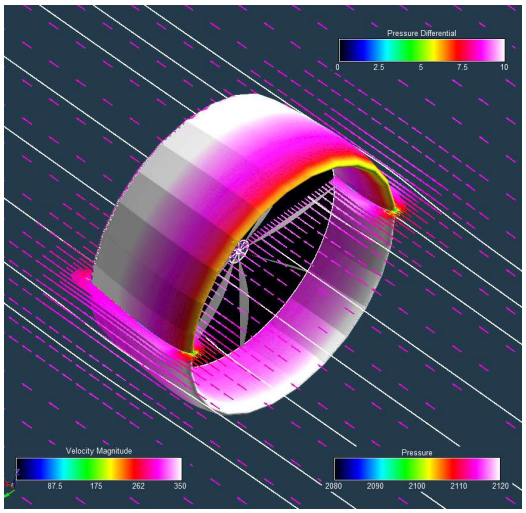

Figure 15. Flow field predictions of the 'baseline' single-fan, circular ducted-fan configuration; freestream velocities of 91 m/s (300 ft/s), collective of 60 deg., nacelle incidence angle of 90 deg.

Figures 16-18 show a representative set of forward flight flow field results for a single circular duct with coaxial fans.

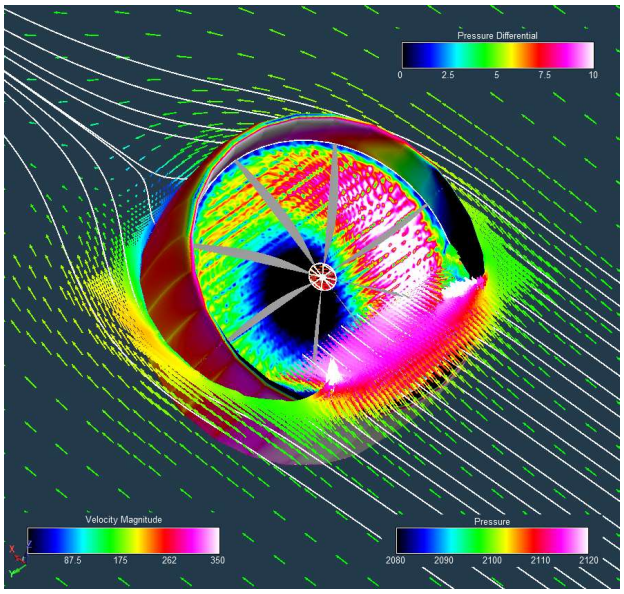

Figure 16. Flow field predictions of the 'baseline' coaxial-fan, circular ducted-fan configuration; freestream velocity of 46 m/s (150 ft/s), collective of 45 deg., nacelle incidence angle of 30 deg.

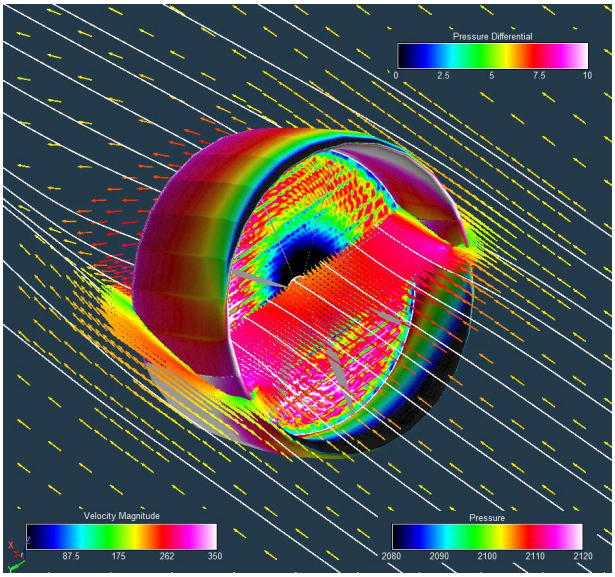

Figure 17. Flow field predictions of the 'baseline' coaxial-fan, circular ducted-fan configuration; freestream velocity of 61 m/s (200 ft/s), collective of 45 deg., nacelle incidence angle of 60 deg.

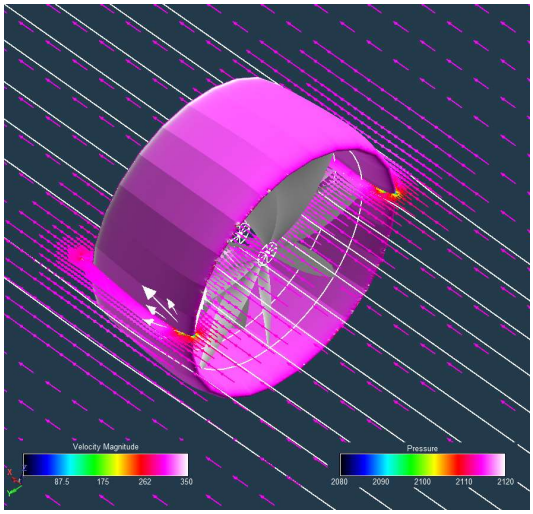

Figure 18. Flow field predictions of the 'baseline' coaxial-fan, circular ducted-fan configuration; freestream velocity of 91 m/s (300 ft/s), collective of 60 deg., nacelle incidence angle of 90 deg.

Figures 19-21 are a set of representative forward flight flow field predictions for an Oval duct configuration (~2R longitudinal fan-to-fan spacing).

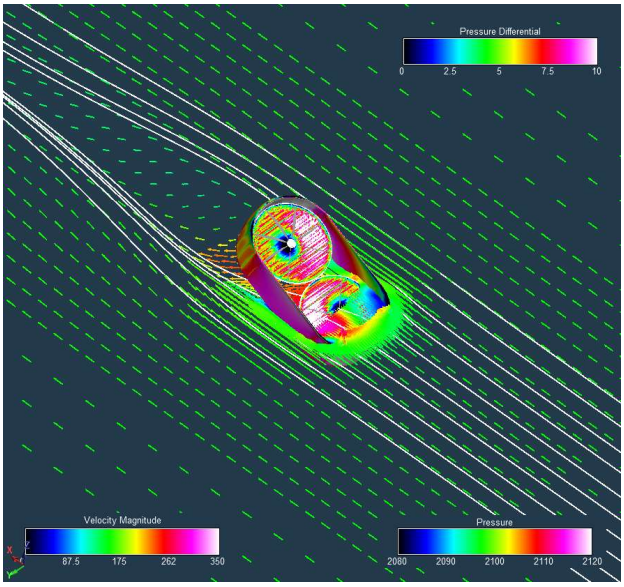

Figure 19. Flow field predictions of the 'baseline' (longitudinal rotor-to-rotor span of 2R) Oval ducted-fan configuration; freestream velocity of 46 m/s (150 ft/s), collective of 45 deg., nacelle incidence angle of 30 deg.

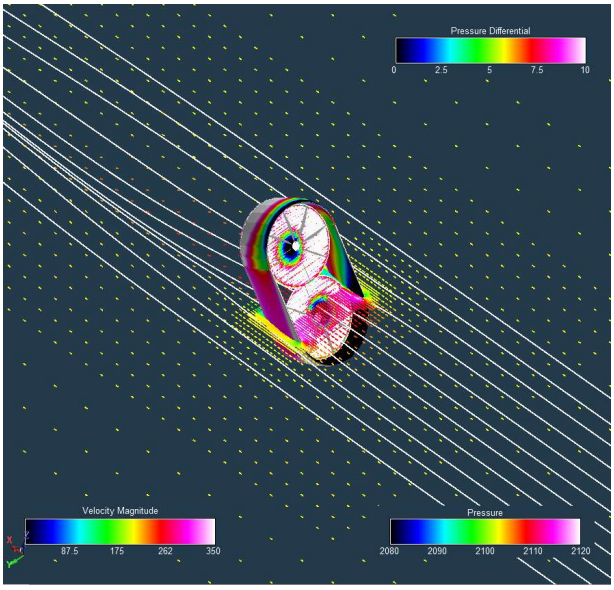

Figure 20. Flow field predictions of the 'baseline' (longitudinal rotor-to-rotor span of 2R) Oval ducted-fan configuration; freestream velocity of 61 m/s (200 ft/s), collective of 45 deg., nacelle incidence angle of 60 deg.

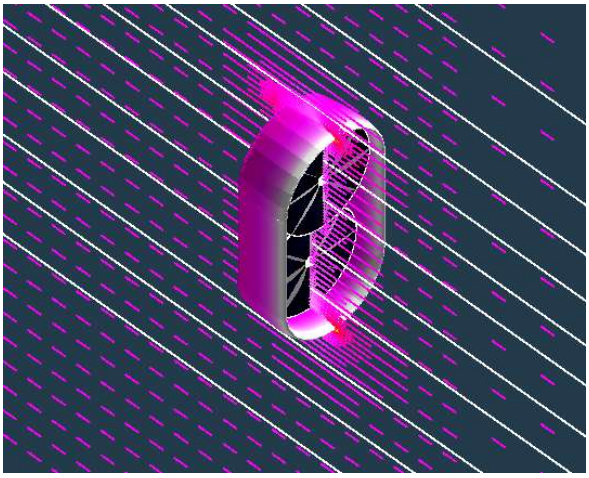

Figure 21. Flow field predictions of the 'baseline' (longitudinal rotor-to-rotor span of 2R) Oval ducted-fan configuration; freestream velocity of 91 m/s (300 ft/s), collective of 60 deg., nacelle incidence angle of 90 deg.

Figures 22-24 are flow predictions of an isolated ducted-fan with the 'baseline' Figure Eight duct configuration. Embedded in the ducted-fan is the tandem fan arrangement. The forward fan is lower in the duct (0.57R below the duct rim/lip) than the aft fan (0.28R below the duct rim lip, for a delta vertical spacing of 0.29R). The Figs. 22-24 results are presented for a 'nominal' prescribed set of flight conditions: (a) freestream velocity of 150 ft/s, collective of 45 deg., nacelle incidence angle of 30 Deg; (b) . freestream velocity of 200 ft/s, collective of 45 deg., nacelle incidence angle of 60 deg.; (c) freestream velocity of 300 ft/s, collective of 60 deg., nacelle incidence angle of 90 deg. These conditions simulate the transition from low-speed flight to cruise speed. These three flight conditions are used for all the forward flight results presented for the baseline Oval, 'Figure Eight,' and 'Figure Bee' isolated duct configurations.

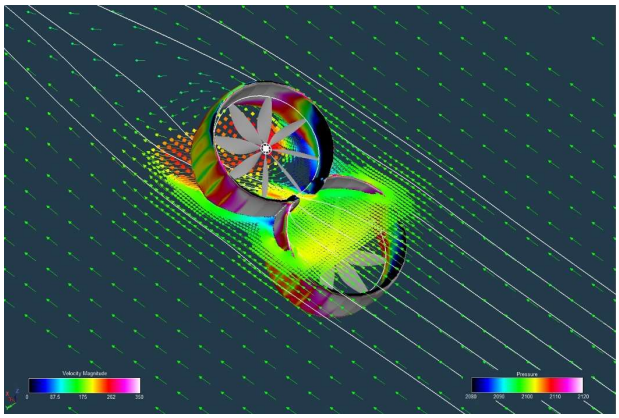

Figure 22. Flow field predictions of the 'baseline' (longitudinal rotor-to-rotor span of 2.1R) isolated 'Figure Eight' ducted-fan configuration; freestream velocity of 46 m/s (150 ft/s), collective of 45 deg., nacelle incidence angle of 30 deg.

In all these transition/cruise forward-flight isolated duct-ed fan configuration results, the velocity magnitude is color-scaled between zero and 100 feet per second. The rotor disk differential pressures are scaled from zero to 10 pounds per square feet. The duct body surface pressures are scaled between 2080 and 2120 pounds per square foot.

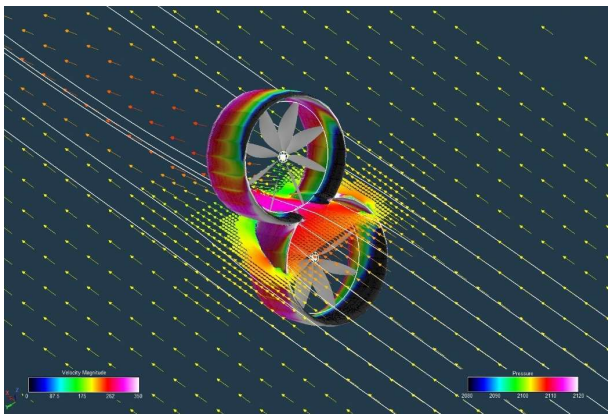

Figure 23. Flow field predictions of the 'baseline' (longitudinal rotor-to-rotor span of 2.1R) isolated Figure Eight ducted-fan configuration; freestream velocity of 61 m/s (200 ft/s), collective of 45 deg., nacelle incidence angle of 60 deg.

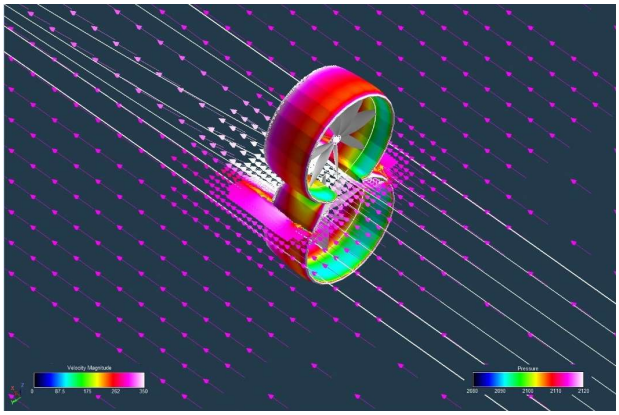

Figure 24. Flow field predictions of the 'baseline' (longitudinal rotor-to-rotor span of 2.1R) isolated Figure Eight ducted-fan configuration; freestream velocity of 91 m/s (300 ft/s), collective of 60 deg., nacelle incidence angle of 90 deg.

Figures 25-27 are a representative set of 'Figure Bee' single duct forward flight flow field predictions. The small channel (~0.25R) between a larger outer side-panel versus a smaller inner side-panel is provided in the Figure Bee configuration to maximize the portion of the circumference of the fans enveloped, or surrounded, by the duct circular arc elements while at the same time allowing for possible wake mixing between the fore and aft duct lobes through the narrow channel formed by the side panels. The influence on thrust augmentation of the relative lateral spacing between the two side panels of Figure Bee type duct configurations will be further explored later in the paper.

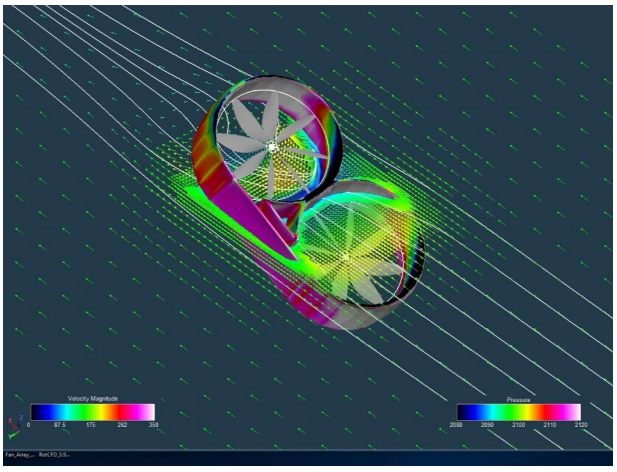

Figure 25. Flow field predictions of the 'baseline' (longitudinal rotor-to-rotor span of 2.1R) 'Figure Bee' ducted-fan configuration; freestream velocity of 46 m/s (150 ft/s), collective of 45 deg., nacelle incidence angle of 30 deg.

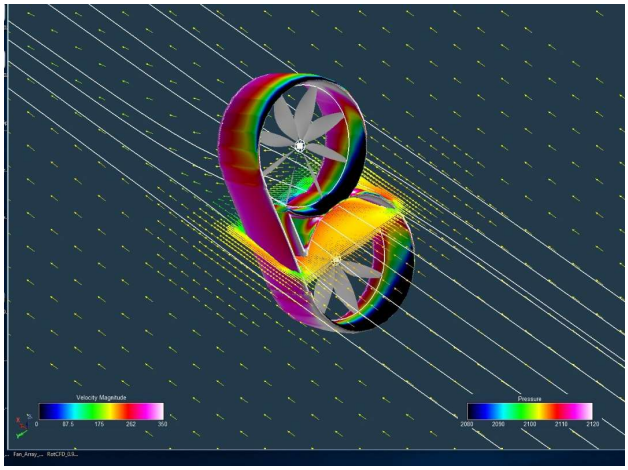

Figure 26. Flow field predictions of the 'baseline' (longitudinal rotor-to-rotor span of 2.1R) 'Figure Bee' ducted-fan configuration; freestream velocity of 61 m/s (200 ft/s), collective of 45 deg., nacelle incidence angle of 60 deg.

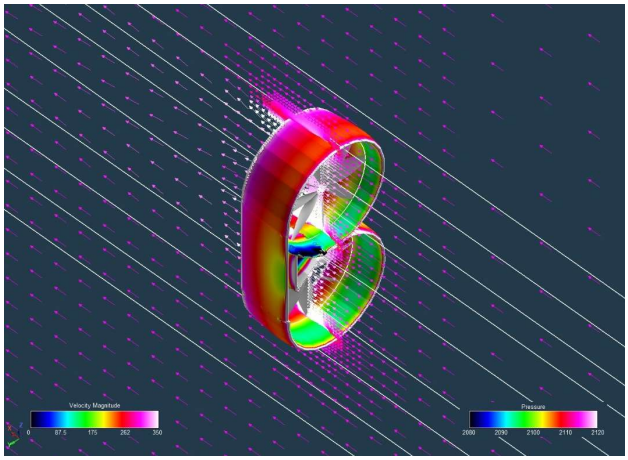

Figure 27. Flow field predictions of the 'baseline' (longitudinal rotor-to-rotor span of 2.1R) 'Figure Bee' ducted-fan configuration; freestream velocity of 91 m/s (300 ft/s), collective of 60 deg., nacelle incidence angle of 90 deg.

Figure 28a-b illustrate the influence on forward flight speed (and attendant nacelle incidence angle and rotor collectives prescribed) on duct lift and drag on the isolated ducted-fans studied. The observed general duct lift and drag coefficient trends, C_L^* and C_D^*, are in general agreement with Eq. 11a-b (modification of the sine-squared formula) used in the sizing analysis presented earlier in the paper. Because the (installed in the duct) fans are not trimmed and only set at generally representative collective settings, rotor transition and cruise thrust and power coefficient CFD predictions under transition and cruise are not presented in this paper.

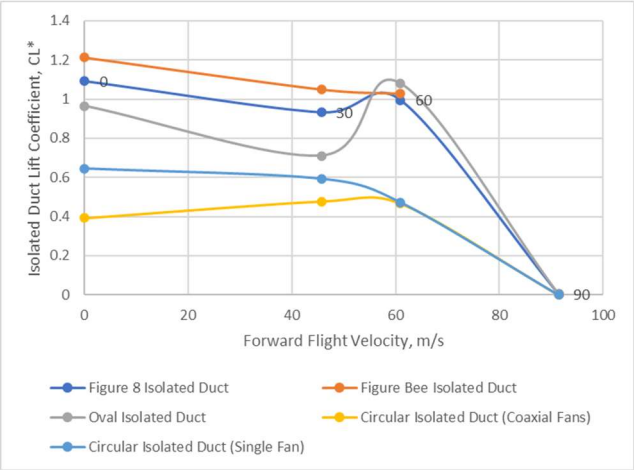

(a)

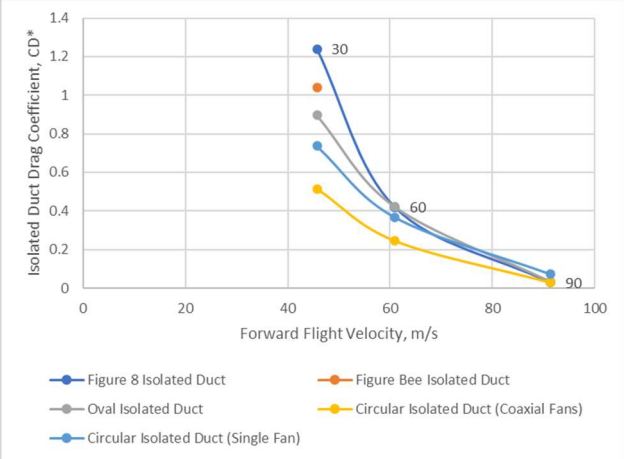

(b)

Figure 28. Duct lift and drag coefficients, C_L^* and C_D^*, for various duct configurations as a function of forward flight speed (and attendant prescribed collective and nacelle incidence angles (shown as data labels))

Predictions from the semi-empirical cruise duct drag formula, Eq. 10, can be compared to some of the RotCFD predictions (fans installed but duct-only forces included). This comparison can be seen in Fig. 29. A reasonably good agreement exists between the RotCFD results and the simple semiempirical model used for duct drag in the sizing analysis.

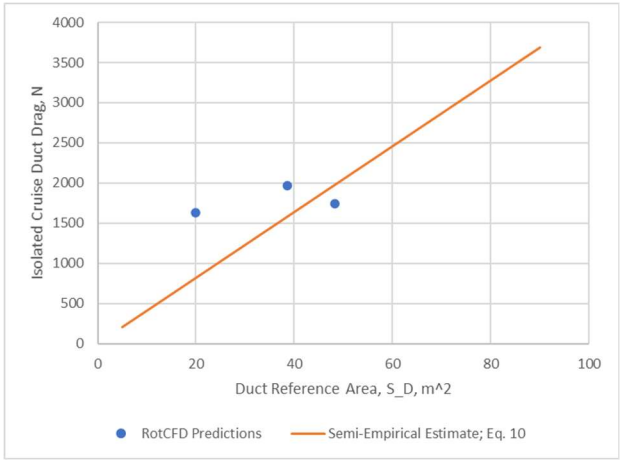

Figure 29. Cruise duct drag comparison (circular duct, oval duct, and Figure Eight in ascending order of duct reference area)

Figures 30-31 examines the aerodynamic impact of parametric geometric changes to the 'baseline' isolated ducted-fan configurations (in hover at a single fan collective setting). Figure 30 shows the impact on duct surface pressures of varying the longitudinal span of Oval ducts. And Fig. 31 shows the impact on duct surface pressures of varying the longitudinal span of a Figure Eight isolated duct configuration.

The aft fan/rotor is to the right-hand side of the images in Figs. 30-31; the forward and lower fan/rotor is on the left-hand-side. The fan disk differential pressures are shown via color mapping in the figures as well as the body surface pressures. As the fan-to-fan longitudinal and lateral spacing is parametrically varied in the below figures, the duct shapes are also changed. Unfortunately, because of the coarseness of the CAD approach to generating the composite (comprised of short side panel linear sections and circular-arc duct segments) duct shapes, the tip gap between the fan tips and the duct interior surfaces was not held constant and varies radially and azimuthally to some degree.

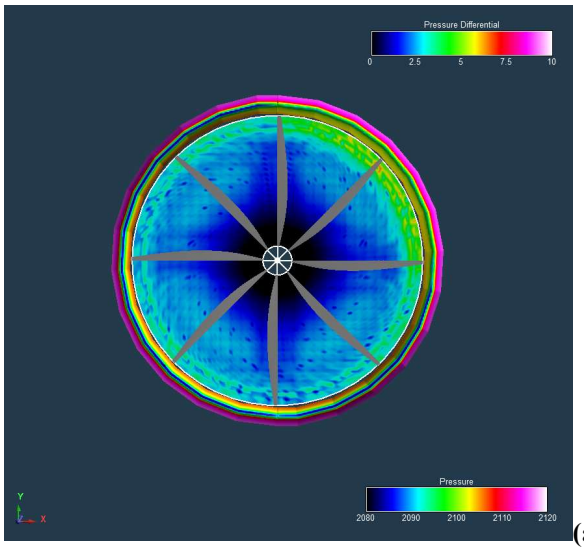

(a)

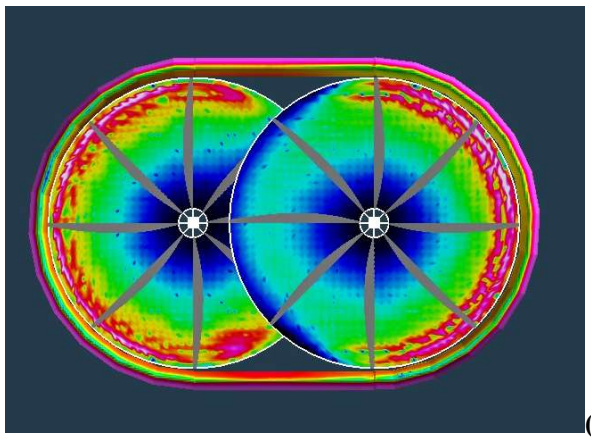
(b)

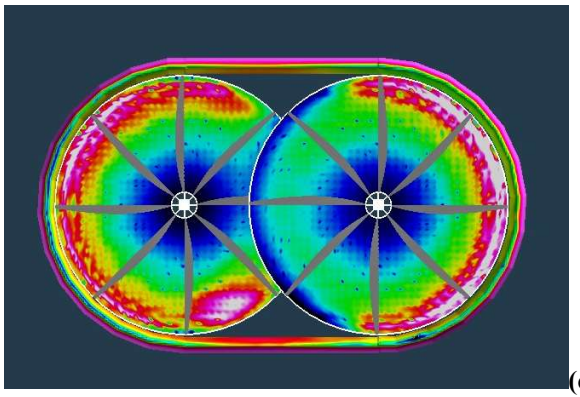
(c)

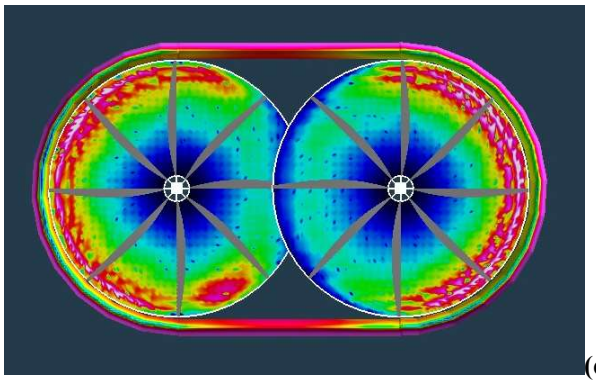
(d)

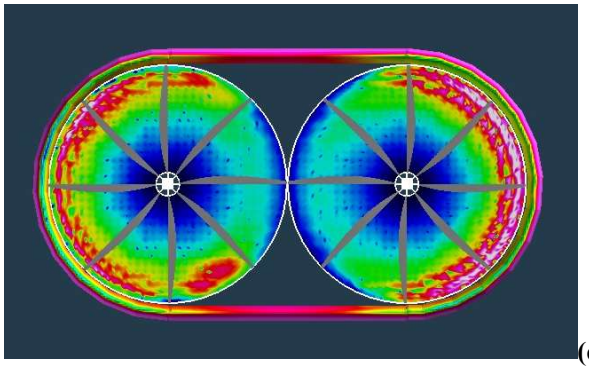
(e)

Figure 30. Oval duct parametric geometry sweep, longitudinal fan-to-fan spacing (15 deg. collective): (a) s/R=0 (circular duct with coaxial fans/rotors); (b) s/R=1.25; (c) s/R=1.5; (d) s/R=1.75; (e) s/R=2

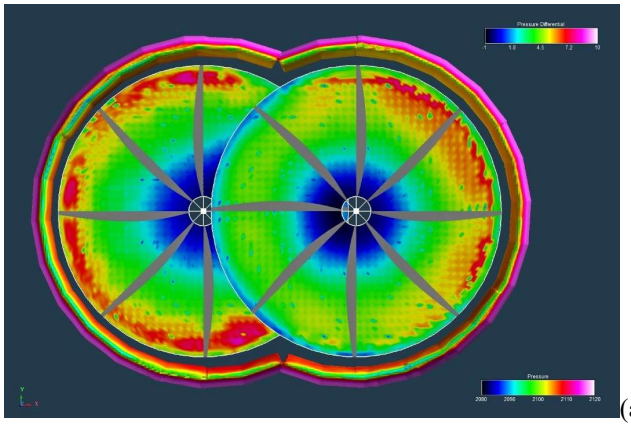
(a)

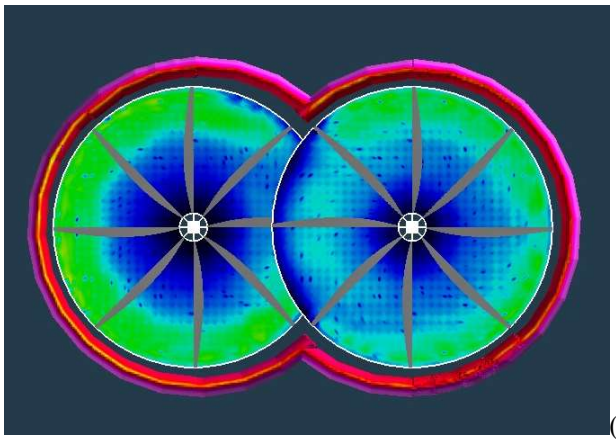

(b)

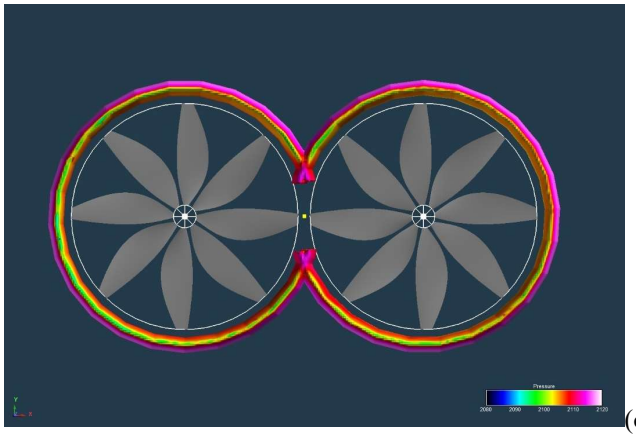

(c)

Figure 31. Parametric geometry sweeps of 'Figure Eight' longitudinal fan-to-fan spacing (s/R); hover predictions at collective of 15 deg: (a) s/R= 1; (b) s/R=1.5; (c) s/R=2.1

Figure 32a-b illustrates the influence on power loading, C_P/C_T and thrust augmentation of the longitudinal spacing, s/R, for the Oval and Figure Eight ducts. Varying the longitudinal fan-to-space spacing – and, therefore, the geometry of the duct – has a small influence on both power loading and thrust augmentation in hover. Though the limited predictions made so far are inadequate to clearly establish overall trends, it is still important to note that fan-to-fan spacing for a given ducted-fan vehicle not going to be dictated by hover performance but by (hover and low-speed pitching-moment) controllability, (cruise) drag, and duct weight considerations.

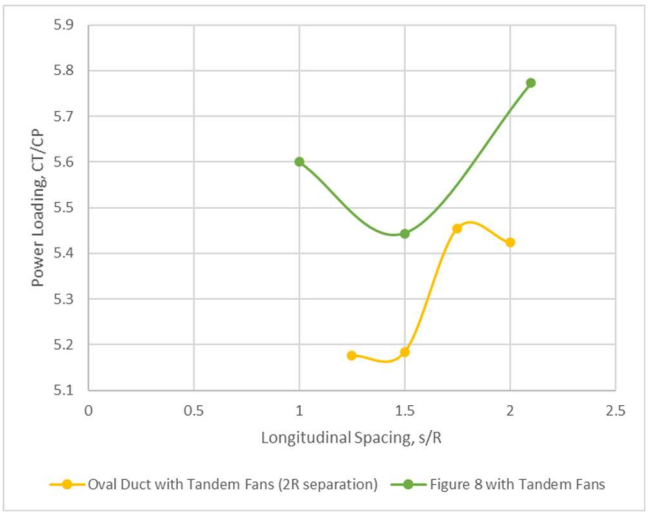

(a)

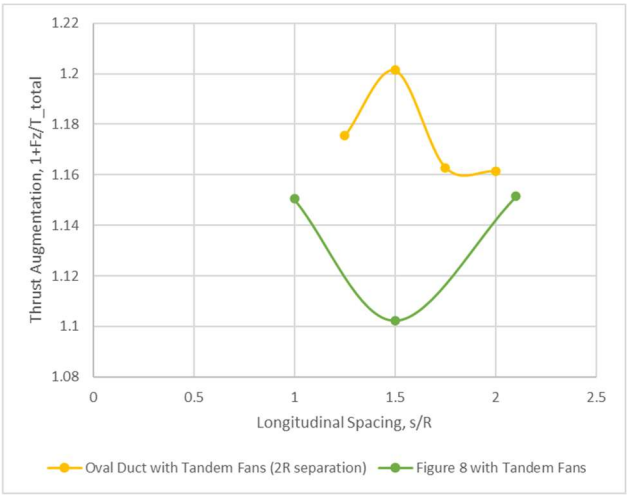

(b)

Figure 32. Influence of longitudinal spacing of fans on ducted-fan geometry, flow field results, hover performance (collective = 15 deg.): (a) power loading and (b) thrust augmentation ratio

Figure 33 illustrates the influence of lateral spacing between an outer side panel (upper panel in figure) and an inner side panel (lower in figure) on duct geometry and flow field predictions. The key outcome of this parametric sweep is primarily introducing a channel formed between the two (inner and outer) side panels that potentially allows induced flow to influence and maybe downstream merge between the two fan wakes. This relative influence (enabled by means of this 'channel' might affect overall duct hover performance.

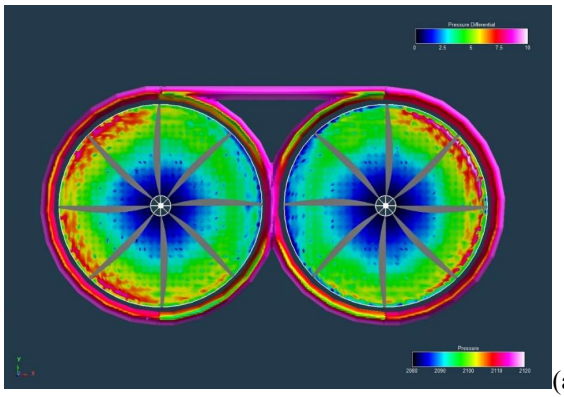
(a)

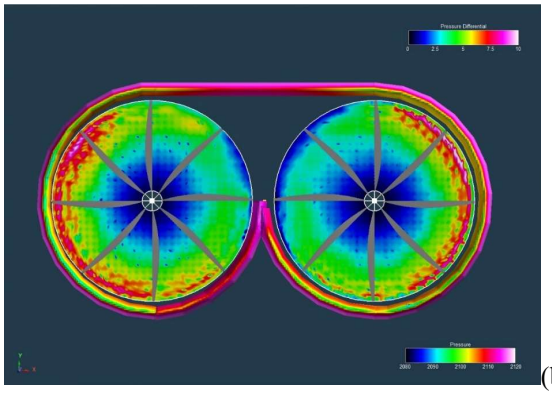
(b)

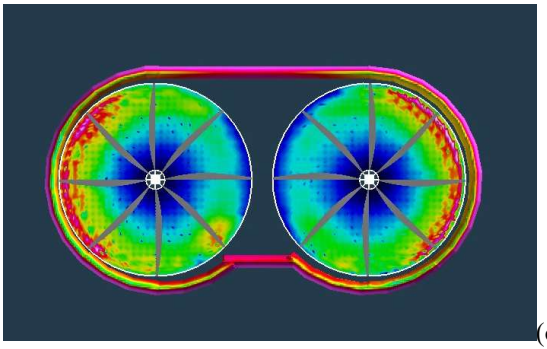
(c)

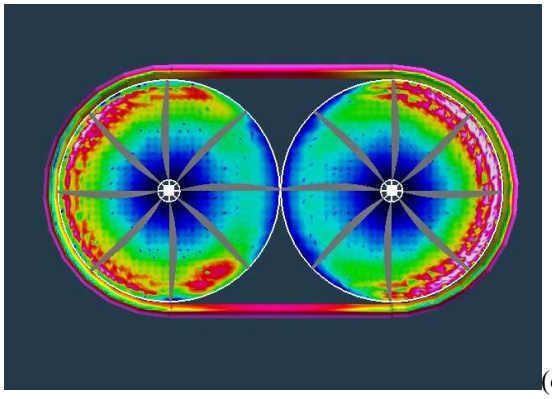
(d)

Figure 33. Parametric geometry sweeps of 'Figure Bee' lateral fan-to-fan spacing (y/R); hover with collective of 15 deg.: (a) y/R=0 (two circular ducts with one long wing side panel spanning across exterior of ducts); (b) y/R=1; (c) y/R=1.8; (d) y/R~2 (oval duct)

Figure 34a-b illustrates the impact on fan power loading and thrust augmentation of the Figure Bee (outer and inner side panel) lateral spacing, y/R. Similar to as was seen for the Oval and Figure Eight ducts and their parametric longitudinal fan-to-fan spacing sweeps, the lateral spacing sweep of the Figure Bee ducts also has a small influence on fan power loading and thrust augmentation. The thrust augmentation values predicted are still overall fairly low, i.e. ~1.15 versus ~1.4 as anticipated from past work in the literature. Improvements in either predictability of thrust augmentation or improved baseline ducted-fan designs will be required to achieve higher thrust augmentation values.

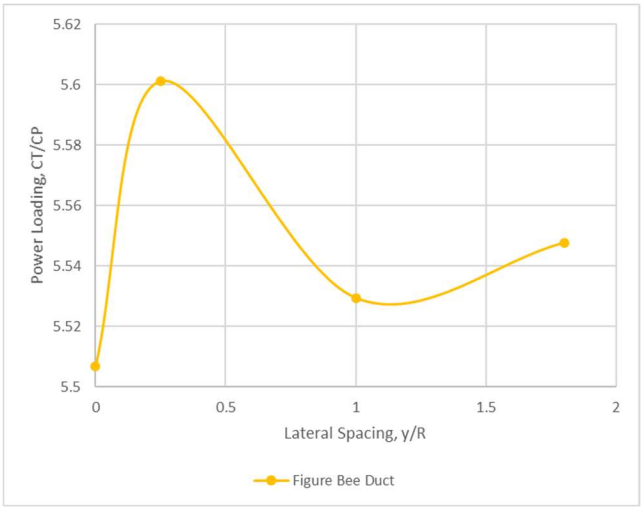

(a)

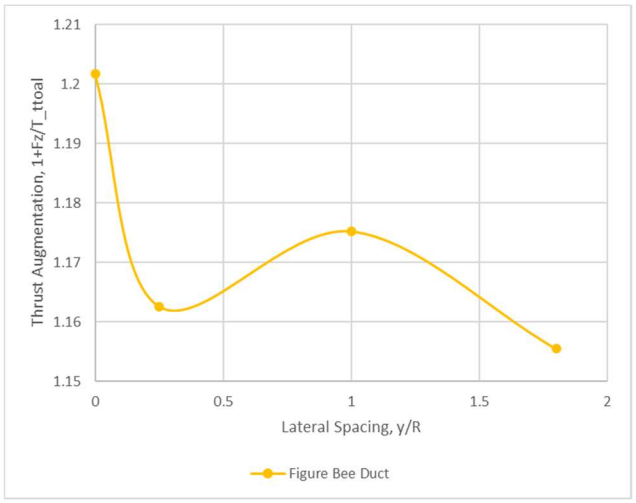

(b)

Figure 34. Hover performance for a range of parametric geometries for Figure Bee duct: (a) power loading and (b) thrust augmentation ratio

Future work will have to be performed to extend the above limited work into the parametric geometry effects on duct hover aeroperformance into forward flight conditions.

Hopefully this limited work to date has shown the flow features and aeroperformance characteristics in common between the circular, Oval, Figure Eight, and Figure Bee ducts. The thrust augmentation due to lip/rim suction pressures (due to the induced/entrained velocity into the duct inlet) should be proportional to first order to the ratio of the ducts' perimeter to the notional circumferences of the (one or two) fans/rotors in the duct, i.e. the ratio of $p/2\pi N_F R_F$. The closer to unity for this ratio, the greater the thrust augmentation for a given mean fan thrust level.

Complete Configuration Predictions

The flow field results of Figs. 35-38 were performed with coarse gridding. This coarse gridding was required to reduce computational resources and required for this preliminary set of results. As such these complete vehicle predictions can be considered only of qualitative value.

The complete vehicle ducted-fan configurations studied include circular ducts, Oval ducts, Figure Eight ducts, and Figure Bee ducts, among others. In the complete vehicle cases presented, coaxial fans of identical geometry, vertical spacing within the ducts, longitudinal fan-to-fan spacing, and collective (15 deg. for hover, 45 deg. for transition, and 60 deg. for cruise) are used for the modeling of the complete vehicles.

Shown in Figs. 35-38 are various velocity vector flow fields (in hover), rotor disk differential pressures (in hover, transition, and cruise), and semi-transparent rotor wake velocity magnitude isosurfaces (for transition and cruise).

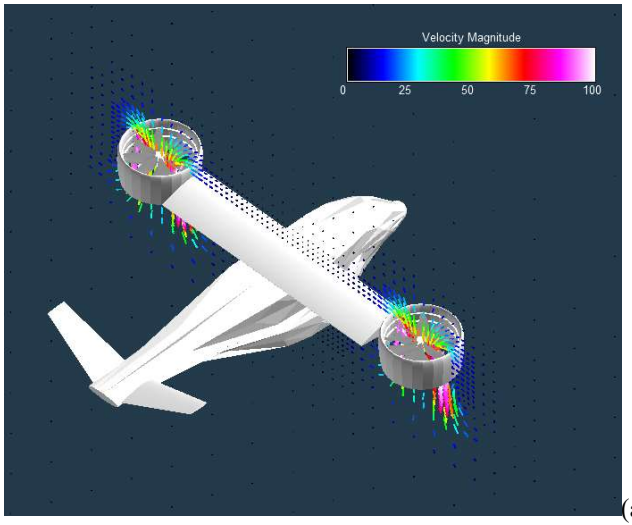

(a)

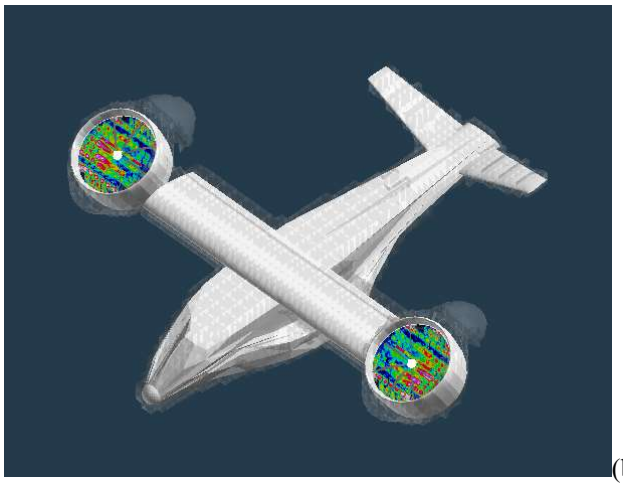
(b)

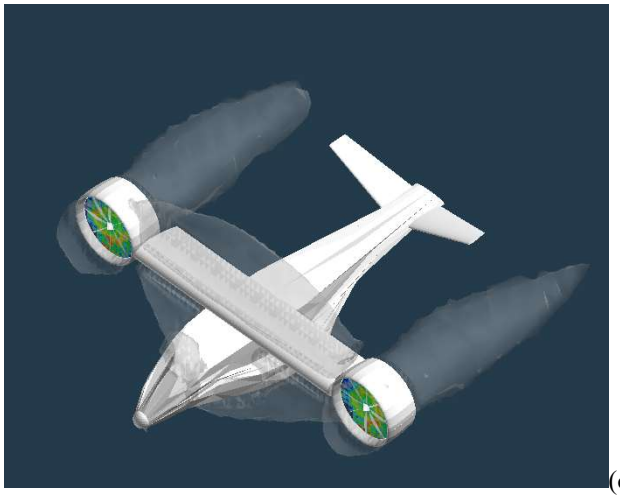
(c)

Figure 35. Aerial Vehicle with tilting circular ducted-fans in (a) hover, (b) transition, and (c) cruise (with mid-fidelity CFD flow field predictions)

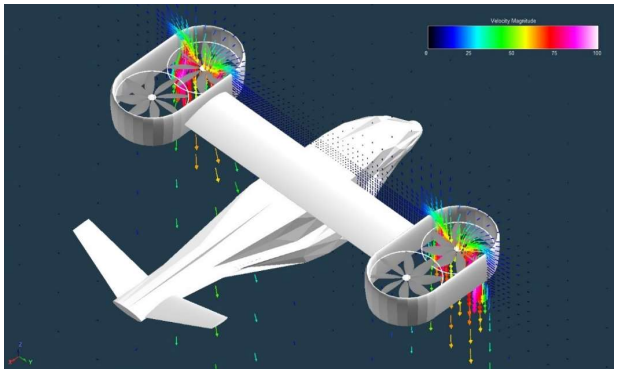
(a)

(b)

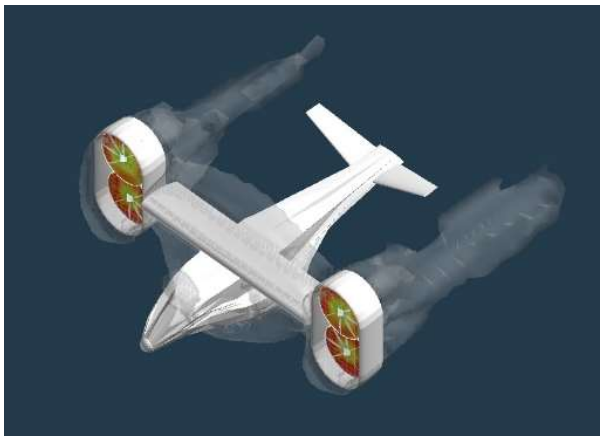

(c)

Figure 36. Aerial vehicle with tilting Oval ducted-fans in (a) hover, (b) transition, and (c) cruise (with mid-fidelity CFD flow field predictions)

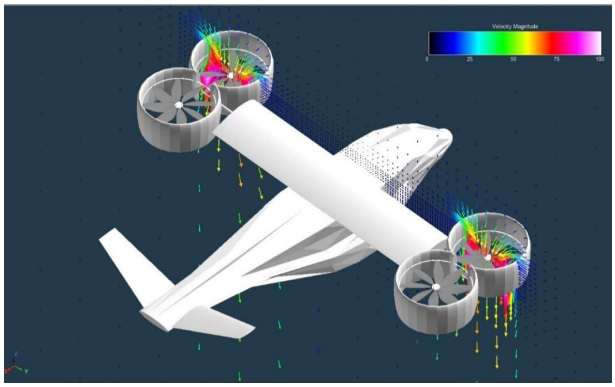

(a)

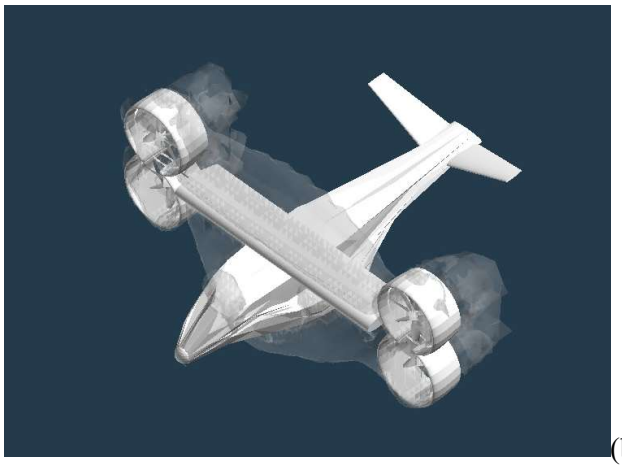

(b)

Figure 37. Aerial vehicle with tilting Figure-Eight ducted-fans in (a) hover and (b) cruise (with mid-fidelity CFD flow field predictions)

This initial complete vehicle work is presented to illustrate some of the major aerodynamic considerations that will need to be performed in future. Chief among these unexplored issues for the future include wing-on-duct and duct-on-wing interactional aerodynamics effects in hover, transition, and cruise. It has been assumed, for example, that tilting ducted-fan vehicles will have lower hover download than comparable tiltrotor aircraft and, perhaps, tiltwing aircraft because of the smaller fan diameters relative to the propellers/proprotors for the other two classes of aircraft. Additionally, one noncircular ducted-fan geometry consideration that needs further exploring is whether a large flat side panel for the ducts for the adjacent region between the ducts and the main wing wingtips is of value in reducing wing/duct junction parasite drag due to adverse interference effects.

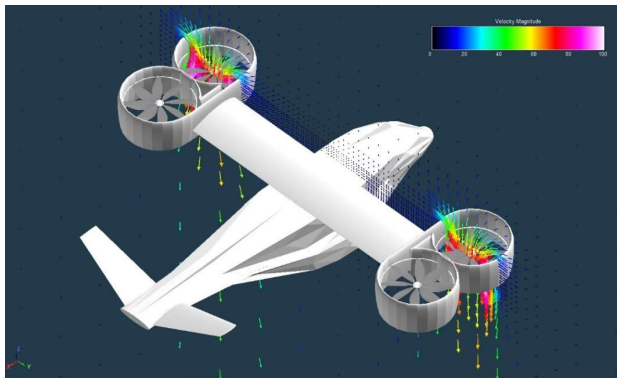

(a)

(b)

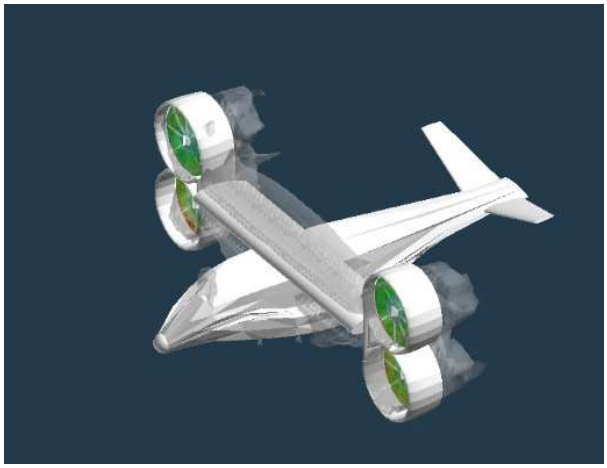

(c)

Figure 38. Aerial vehicle with tilting Figure Bee ducted-fans in (a) hover, (b) transition, and (c) cruise (with mid-fidelity CFD flow field predictions)

FUTURE WORK INTO MISC. AERODYNAMIC CONSIDERATIONS

In addition to relying upon differential thrust between fore and aft rotors/fans in the ducted-fans for vehicle pitching moment control, it might be necessary to also accommodate nacelle fans as has been proposed for previous tilting-ducted-fan VTOL aircraft. The relative control effectiveness of differential thrust versus nacelle vanes is a largely unexplored design trade that will have to be performed in future work. Figure 39a-b presents some preliminary work on nacelle vanes in oval ducts in hover. Considerably more work will be required to arrive at satisfactory control/design solutions.

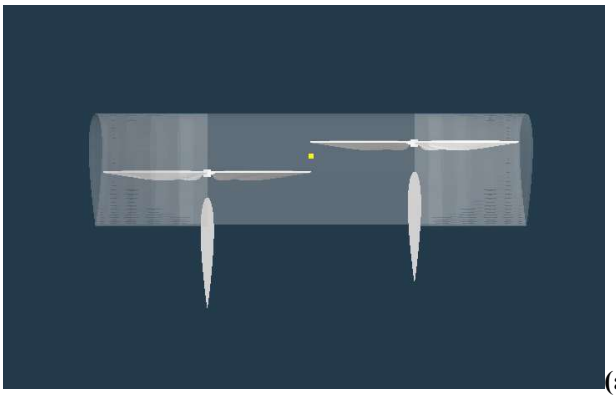

(a)

(b)

Figure 39. Nacelle control vanes in Oval ducts: (a) side ('cutaway') view and (b) isometric view

Additional miscellaneous aerodynamic work left for the future includes the utility of small vortex generators and splitter vanes in duct interiors to enhance internal duct flow missing and, therefore, improve overall thrust augmentation in hover and reduced duct parasite drag in cruise (e.g. refer to the discussion in Ref. 26).

CONCLUDING REMARKS

This paper focused on aerodynamic and conceptual design questions related to novel tilting ducted-fan (wing-mounted) aerial vehicle configurations. Only a relatively few urban air mobility (UAM) aircraft concepts have been proposed for this general type of VTOL aircraft.

A simple sizing analysis was presented for tilting ducted-fan aircraft responding to UAM type mission profiles. Additionally, a preliminary set of mid-fidelity computational

fluid dynamic analyses were also performed for tilting ducted-fan configurations.

The different noncircular ducts considered in the sizing analysis yielded a 150% in duct reference area from a circular duct but yielded only a 20% growth in resulting tilting ducted-fan vehicle design gross weight (for all-electric battery propulsion systems) for the UAM mission application studied. Weight growth trends for noncircular ducts should in the future be considered for vehicles with hybrid-electric and turboshaft propulsion systems; the anticipation is that there might be a smaller weight growth trend with noncircular ducts.

The mid-fidelity CFD work focused primarily on isolated (single) ducted fan configurations. A limited number of complete vehicle predictions were also performed, with relatively coarse grids, and used to merely demonstrate some of the challenges to be faced for duct-on-wing and wing-on-duct aerodynamic interactions. For the isolated ducted fan configurations, both flow field and aeroperformance results were predicted and presented for all phases of flight, including hover, transition, and cruise. The focus of these mid-fidelity CFD predictions was to examine fan-on-duct and duct-on-fan aerodynamic interactions. In particular, examining fan thrust augmentation in hover, as a function of noncircular duct geometries relative to circular ducts, was a key consideration in this work. Overall, all noncircular ducts had less thrust augmentation than circular ducts but slight but important geometry effects were noted where some noncircular geometries performed better than others. Additionally, the predicted hover thrust augmentation is lower than what historical data from the literature would suggest is possible for ducted-fan vehicles. However, the relatively low fan disk loadings (~960N/m^2 or ~20psf) studied in this paper could influence some of the observations made; it is potentially important for future work to examine ducted-fans with higher disk loadings. Overall, this combined conceptual design sizing analysis and CFD exercise should be considered a preliminary effort to understand a potentially important vehicle type for UAM mission applications.

It is hoped that this work will ultimately lead to design and technology advances that will result in expanded roles for tilting ducted-fan aircraft for not only UAM-type missions but terrestrial UAV/drone missions, and possibly planetary science missions (particularly, those related to possible future exploration of Titan, a moon of Saturn).

Author contact: Larry A, Young larry.a.young@nasa.gov

ACKNOWLEDGMENTS

The author would like to acknowledge the work in the early 2000's on tilting ducted-fan and planetary aerial vehicles of Edwin Aiken (Ret.), Mike Derby, Jeff Johnson, and Ray Demblewski of the NASA Ames Research Center (at the time of the original work). Additionally, the contributions to the powered-lift research community of the late Michael Dudley, NASA Ames Research Center, is also acknowledged.

REFERENCES

1. Doak VZ-4; https://en.wikipedia.org/wiki/Doak_VZ-4; last accessed December 9, 2022.
2. Doak VZ-4DA Flight Demonstrator; https://vertipedia.vtol.org/aircraft/getAircraft/aircraftID/374; last accessed December 10, 2022.
3. Bell X-22; https://en.wikipedia.org/wiki/Bell_X-22; last accessed December 9, 2022.
4. Eskey, M. and Wilson, III, S., "The Handling Qualities and Flight Characteristics of the Grumman Design 698 Simulated Twin-Engine Tilt Nacelle V/STOL Aircraft," NASA TM 86785, June 1986.
5. Bell Nexus Air Taxi vehicle concept; https://www.bellflight.com/products/bell-nexus; last accessed December 25, 2022.
6. Airbus Cityairbus concept and demonstrator; https://www.airbus.com/en/urbanairmobility/cityairbus-nextgen/cityairbus-demonstrator; last accessed December 9, 2022.
7. Vertical Flight Society eVTOL Aircraft Directory; https://evtol.news/aircraft; last accessed December 26, 2022.
8. Patterson, M. D., Antcliff, K. R., and Kohlman, L. W., "A Proposed Approach to Studying Urban Air Mobility Missions Including an Initial Exploration of Mission Requirements," AHS International 74th Annual Forum, AHS International, Phoenix, 2018.
9. Young, L.A., Aiken, E.W., Derby, M.R., Johnson, J.L., Navarrete, J., and Demblewski, R., "Engineering Studies into Vertical Lift Planetary Aerial Vehicles," AHS International Meeting on Advanced Rotorcraft Technology and Life Saving Activities, Utsunomiya, Tochigi, Japan, November 11-13, 2002.
10. Russell, C.R.; Young, L.A.; Yamauchi, G.K.; Johnson, W.; Boyd, D.D.; Gorton, S.A.; Snyder, C.A.; and Kohlman, L.W.: Greener Helicopters. Encyclopedia of Aerospace Engineering, eds R. Blockley and W. Shyy, John Wiley: Chichester. DOI: 10.1002/9780470686652.eae1009. Published 12/29/2015.
11. Alonso, J.J., Arneson, H.M., Melton, J.E., Vegh, J.M., Walker, C., and Young, L.A., "System-of-Systems Considerations in the Notional Development of a Metropolitan Aerial Transportation System: Implications as to the Identification of Enabling Technologies and Reference Designs for Extreme Short Haul VTOL Vehicles with Electric Propulsion," NASA TM 2017-218356, September 2017.
12. Young, L.A., "Accessibility Design and Operational Considerations for Urban Aerial Mobility Vehicles and Networks," Vertical Flight Society (VFS)

Transformative Vertical Flight 2020: International Power Lift Conference (IPLC), San Jose, CA, January 21-23, 2020.
13. Young, L.A., “Urban Aerial Mobility Networks using Amphibious Vertical Takeoff and Landing Vehicles,” 9th Biennial Autonomous VTOL Technical Meeting & 8th Annual Electric VTOL Symposium, Jan. 26–28, 2021.
14. Young, L.A., “A Transportation and Habitation System Architecture enabled by Multi-Modality Mobility Platforms,” NASA TM (Soon to be published).
15. Whiteside, S. and Pollard, B., “Conceptual Design of a Tiltduct Reference Vehicle for Urban Air Mobility, VFS Aeromechanics for Advanced Vertical Flight Technical Meeting, San Jose, CA, Jan 25-27, 2022.
16. Chung, W.W., Paris, A., Salvano, D., Linse, D., Trept, T., Wood, T., Young, R., Gao, H., Wright, K., Miller, D., Cheng, V. “Modeling High-Speed Civil Tiltrotor Transports in the Next Generation Airspace”, Volume II, NASA CR-2011-215960.
17. Acree, C. and Snyder, C., “Influence of Alternative Engine Concepts on LCTR2 Sizing and Mission Profile”, AHS Future Vertical Lift Aircraft Design Conference, January 18-20, 2012 San Francisco, CA.
18. Johnson, W., Yamauchi, G. K. and Watts, M. E., "Designs and Technology Requirements for Civil Heavy Lift Rotorcraft," Proceedings of the American Helicopter Vertical Lift Aircraft Design Conference, San Francisco, CA, January 18-20, 2006.
19. Wilkerson, J.B., and Smith, R.L., “Aircraft System Analysis of Technology Benefits to Civil Transport Rotorcraft,” NASA/CR-2008-214594, 2008.
20. Stepniewski, W.Z., and Shinn, R.A., “A Comparative Study of Soviet vs. Western Helicopters,” NASA CR 3579, CR 3580, March 1983.
21. Tishchenko, M.N.; Nagaraj, V.T.; and Chopra, I. “Preliminary Design of Transport Helicopters.” Journal of the American Helicopter Society, Vol. 48, No. 2, April 2003.
22. Johnson, W., "NDARC: NASA Design and Analysis of Rotorcraft Theory," NASA/TP–20220000355, Vol. 1.
23. Radotich, M., "Conceptual Design of Tiltrotor Aircraft for Urban Air Mobility," Presented at the VFS Aeromechanics for Advanced Vertical Flight Technical Meeting, San Jose, CA, Jan 25-27, 2022.
24. Rajagopalan, R.G., Baskaran,V., Hollingsworth, A., Lestari, A., Garrick, D., Solis, E., Hagerty, B., “RotCFD - A Tool for Aerodynamic Interference of Rotors: Validation and Capabilities”, AHS Future Vertical Lift Aircraft Design Conference, January 18-20, 2012 San Francisco.
25. Rajagopalan, G., Thistle, J., Polzin, W., "The Potential of GPU Computing for Design in RotCFD," AHS Technical Meeting on Aeromechanics Design for Vertical Lift, Holiday Inn at Fisherman's Wharf, San Francisco, CA, January 16-18, 2018.
26. Young, L.A., “Conceptual Design Aspects of Three General Sub-Classes of Multi-Rotor Configurations: Distributed, Modular, and Heterogeneous,” Sixth AHS International Specialists Meeting on Unmanned Rotorcraft Systems, Scottsdale, AZ, January 20-22, 2015.